CHAPTER

6

Cooperative Object Manipulation and Control

6.1 INTRODUCTION

The problem of multiarm and multirobot cooperation is similar to the problem of multifinger grasping. The main difference is in the modeling of the contacts between the fingertips (or the hands) and the object.

When a hand grasps an object, the contacts established between the fingers and the object are generally unilateral. As discussed in Section 2.9.3, the transmission of velocities and angular velocities (twists) between the fingers and the object is represented by velocity transform bases $\mathbb{B}_m$. The transmission of forces and moments (wrenches), on the other hand, is represented by constraint bases $\mathbb{B}_c$.

In the discussion about multiarm and multirobot cooperation, it is assumed that the robot hands grasp the object firmly. Hence, each robot hand can apply a 6-DoF wrench to the object. Therefore, the respective velocity transform basis $\mathbb{B}_m$ becomes a zero matrix, while the constraint basis $\mathbb{B}_c$ becomes a 6D identity matrix.

In multifinger grasping and multiarm and multirobot cooperation, the grasped object may deform. Since the aim in the following discussion, however, is to better understand the basics of grasping and cooperation, it will be assumed that the object does not deform.

The chapter is structured as follows. Section 6.2 discusses multifinger grasping. The ability of a grasp to resist external wrenches applied to the grasped object deeply depends on the type of grasping. The grasping ability can be characterized with the help of the *form closure* and *force closure* concepts. These concepts make use of the grasp and hand Jacobian matrices and of the kinematics relationship between the fingertips and the object. At the end of the section, simple examples for better understanding will be presented.

Section 6.3 discusses the problem of multiarm cooperation. There are two major approaches: master-slave and symmetry-type cooperation. When p robot arms grasp an object, the arms can apply $6p$-dimensional wrenches to the object in total. Among the $6p$-dimensional wrenches, a 6D wrench is used to control the external wrench. The remaining $6(p-1)$-dimensional wrenches are used to control the internal wrenches. The methods used to control external and internal wrenches are discussed in this section as well.

In Section 6.4, multirobot cooperation is discussed. It is worth noting that when multiple wheeled robots cooperate, the so-called "leader-follower"-type cooperation is widely used. This type of cooperation, however, is not suitable when multiple legged robots cooperate

https://doi.org/10.1016/B978-0-12-804560-2.00013-4

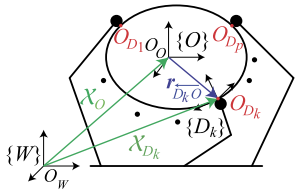

FIGURE 6.1 The object is grasped by p robot fingers.

since there will be a time lag between the motion of the leader and that of the followers. The time lag may cause the robots to fall down. In multirobot cooperation, the so-called "symmetry"-type cooperation is more suitable; it can be expected that all robots move synchronously, and hence, no internal wrenches will be generated in the ideal case. Therefore, the focus in Section 6.4 is on the symmetry-type cooperation.

The problem of dynamic object manipulation is highlighted in Section 6.5.

6.2 MULTIFINGER GRASPING

This section discusses mainly the ability of a robotic hand to resist external wrenches applied to the grasped object. The ability of the hand to resist the external wrenches is characterized by two concepts: the *form closure* and the *force closure*. The terms *form closure* and *force closure* originally appeared in [20] and were used to represent constraint conditions. Partial form and force closure properties of grasping were discussed in [2].

Several different types of finger contacts have been modeled so far. Some examples from the taxonomy of contacts are: (1) lack of contact (six freedoms), (2) point contact without friction (five freedoms), (3) line contact without friction (four freedoms), (4) point contact with friction (three freedoms), (5) planar contact without friction (three freedoms), (6) soft finger (two freedoms), (7) line contact with friction (one freedom), and (8) planar contact with friction (0 freedoms) [15]. Among the above finger contact models, three contact models, (2) point contact without friction, (4) point contact with friction, and (6) soft finger, are most common [21]. This section deals with these three contact models to analyze closure properties.

6.2.1 Grasp Matrix and Hand Jacobian Matrix

Motion constraints through contacts were presented in Section 2.9. Suppose that p robot fingers grasp an object as illustrated in Fig. 6.1. Let $\{O\}$, $\{D_k\}$, and $\{W\}$ be coordinate frames fixed on the object, at the kth contact point between a finger and the object, and the inertial coordinate frame, respectively. The axes of frame $\{D_k\}$ are defined so that the z-axis is normal to the contact surface and points to the interior of the object. The other two axes are orthogonal and lie in the tangential plane (see Fig. 6.2). The origin of frame $\{D_k\}$, O_{D_k}, is placed at the contact point in case of a point contact, or at the center of pressure (CoP) in the case of a plane or line contact. The terms O_O and O_W denote the origins of coordinate frames $\{O\}$ and $\{W\}$, respectively. In general, O_O can be any point on the object. The preferable choice, however, is

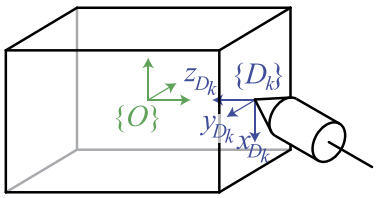

FIGURE 6.2 Contact coordinate frame $\{D_k\}$.

at the center of mass (CoM) since in this case, a force applied along $\boldsymbol{r}_{\overleftarrow{D_k O}}$ (see Fig. 6.1) will not produce a moment about the CoM. Thus, the equation of motion will be simple. Note that in the above figures and throughout this chapter, the j subscript will be used to indicate the number of the finger (or arm).[1] The terms $\mathcal{X}_O$ and $\mathcal{X}_{D_k}$ denote the 6D position (position and orientation) of the object at O_O and O_{D_k}, respectively, with respect to $\{W\}$.

The number of motion constraints at each contact joint is denoted as c_j (< 6) as defined in Section 2.9. The case of $c_j = 6$ will be described in Section 6.3; $\boldsymbol{r}_{\overleftarrow{D_k O}}$ is a 3D vector pointing from O_O to O_{D_k} with respect to $\{W\}$.

Let $\mathcal{V}_O = \begin{bmatrix} \boldsymbol{v}_O^T & \boldsymbol{\omega}_O^T \end{bmatrix}^T$ and ${}^{D_k}\mathcal{V}_{D_k}^O = \begin{bmatrix} {}^{D_k}\boldsymbol{v}_{D_k}^T & {}^{D_k}\boldsymbol{\omega}_{D_k}^T \end{bmatrix}^T$ be the translational and angular velocities (twists) (see Section 2.4) of the object at O_O with respect to $\{W\}$ and at contact point $\mathcal{X}_{D_k}$ with respect to $\{D_k\}$, respectively. The relationship between $\mathcal{V}_O$ and ${}^{D_k}\mathcal{V}_{D_k}^O$ is given by

$$ {}^{D_k}\mathcal{V}_{D_k}^O = {}^{D_k}\mathbb{X}_{W_{\overleftarrow{D_k O}}} \mathcal{V}_O, \tag{6.1} $$

where

$$ {}^{D_k}\mathbb{X}_{W_{\overleftarrow{D_k O}}} = \begin{bmatrix} \boldsymbol{R}_{D_k}^T & \boldsymbol{0}_3 \\ \boldsymbol{0}_3 & \boldsymbol{R}_{D_k}^T \end{bmatrix} \begin{bmatrix} \boldsymbol{E}_3 & -\left[\boldsymbol{r}^{\times}_{\overleftarrow{D_k O}}\right] \\ \boldsymbol{0}_3 & \boldsymbol{E}_3 \end{bmatrix} = \begin{bmatrix} \boldsymbol{R}_{D_k}^T & -\boldsymbol{R}_{D_k}^T \left[\boldsymbol{r}^{\times}_{\overleftarrow{D_k O}}\right] \\ \boldsymbol{0}_3 & \boldsymbol{R}_{D_k}^T \end{bmatrix} \in \Re^{6\times 6} \tag{6.2} $$

is the twist transform matrix from $\mathcal{V}_O$ to ${}^{D_k}\mathcal{V}_{D_k}^O$; $\boldsymbol{R}_{D_k}$ is the rotation matrix that represents the orientation of $\{D_k\}$ with respect to $\{W\}$, ${}^{D_k}\mathbb{X}$ is called *partial grasp matrix* [24].

Let ${}^{D_k}\mathcal{V}_{D_k}^l$ be the twist of the finger at contact point $\mathcal{X}_{D_k}$ with respect to $\{D_k\}$; ${}^{D_k}\mathcal{V}_{D_k}^l$ is given as follows:

$$ {}^{D_k}\mathcal{V}_{D_k}^l = {}^{D_k}\boldsymbol{J}(\boldsymbol{\theta}_{D_k})\dot{\boldsymbol{\theta}}_{D_k}, \tag{6.3} $$

where ${}^{D_k}\boldsymbol{J}$ is the finger Jacobian matrix defined in $\{D_k\}$ and $\boldsymbol{\theta}_{D_k}$ is the joint angle vector of the finger in contact with the object at O_{D_k}.

Contact joint models were described in Section 2.9.3. The velocities of the object and the finger in contact are constrained at O_{D_k}. The motion constraint of the object and the finger at

[1] In other chapters of this work (e.g. in Chapter 2) the j subscript is used to indicate l (left) or r (right).

contact point O_{D_k} is given by

$$ {}^{D_k}\mathbb{B}_c^T \left({}^{D_k}\mathcal{V}_{D_k}^l - {}^{D_k}\mathcal{V}_{D_k}^O \right) = \mathbf{0}_{c_j}, \tag{6.4} $$

where ${}^{D_k}\mathbb{B}_c \in \Re^{6\times c_j}$ is the constraint basis at contact point O_{D_k} with respect to $\{D_k\}$. See Section 2.10.1 for motion analysis of closed loop chains.

The twists of the object and the finger, ${}^{D_k}\mathcal{V}_{D_k}^O$ and ${}^{D_k}\mathcal{V}_{D_k}^l$, for $k = 1, \cdots, p$, are combined into ${}^C\mathcal{V}_C^O$ and ${}^C\mathcal{V}_C^l$, respectively, as follows:

$$ {}^C\mathcal{V}_C^O = \begin{bmatrix} {}^{D_1}\mathcal{V}_{D_1}^O \\ \vdots \\ {}^{D_p}\mathcal{V}_{D_p}^O \end{bmatrix}, \quad {}^C\mathcal{V}_C^l = \begin{bmatrix} {}^{D_1}\mathcal{V}_{D_1}^l \\ \vdots \\ {}^{D_p}\mathcal{V}_{D_p}^l \end{bmatrix}. \tag{6.5} $$

Here ${}^C\mathcal{V}_C^O$ and ${}^C\mathcal{V}_C^l$ are given by

$$ {}^C\mathcal{V}_C^O = {}^C\mathbb{X}\mathcal{V}_O, \tag{6.6} $$

$$ {}^C\mathcal{V}_C^l = {}^C\boldsymbol{J}\,(\boldsymbol{\theta}_C)\,\dot{\boldsymbol{\theta}}_C, \tag{6.7} $$

where

$$ {}^C\mathbb{X} = \begin{bmatrix} {}^{D_1}\mathbb{X} \\ \vdots \\ {}^{D_p}\mathbb{X} \end{bmatrix}, \quad {}^C\boldsymbol{J} = \begin{bmatrix} {}^{D_1}\boldsymbol{J} & & \mathbf{0} \\ & \ddots & \\ \mathbf{0} & & {}^{D_p}\boldsymbol{J} \end{bmatrix}, \quad \boldsymbol{\theta}_C = \begin{bmatrix} \boldsymbol{\theta}_{D_1} \\ \vdots \\ \boldsymbol{\theta}_{D_p} \end{bmatrix}. $$

The total motion constraints are described as follows:

$$ {}^C\mathbb{B}_c^T \left({}^C\mathcal{V}_C^l - {}^C\mathcal{V}_C^O \right) = \mathbf{0}_c, \tag{6.8} $$

where

$$ c = \sum_{j=1}^{p} c_j \quad \text{and} \quad {}^C\mathbb{B}_c^T = \begin{bmatrix} {}^{D_1}\mathbb{B}_c^T & & \mathbf{0} \\ & \ddots & \\ \mathbf{0} & & {}^{D_p}\mathbb{B}_c^T \end{bmatrix} \in \Re^{c\times 6p}. $$

Eq. (6.8) can be rewritten in a matrix form as

$$ \begin{bmatrix} -{}^C\boldsymbol{G}^T & {}^C\boldsymbol{J} \end{bmatrix} \begin{bmatrix} \mathcal{V}_O \\ \dot{\boldsymbol{\theta}}_C \end{bmatrix} = \mathbf{0}_c, \tag{6.9} $$

$$ {}^C\boldsymbol{G}^T \equiv {}^C\mathbb{B}_c^T {}^C\mathbb{X} \in \Re^{c\times 6}, $$

$$ {}^C\boldsymbol{J} \equiv {}^C\mathbb{B}_c^T {}^C\boldsymbol{J} \in \Re^{c\times n_{\theta_c}}, $$

where n_{θ_c} is the dimension of $\boldsymbol{\theta}_C$; ${}^C\boldsymbol{G}$ and ${}^C\boldsymbol{J}$ are called *grasp matrix* and *hand Jacobian*, respectively [24].

6.2.2 Statics of Grasping

Eq. (6.9) is rewritten as follows:

$$ {}^{C}\boldsymbol{G}^{T}\mathcal{V}_{O} = {}^{C}\boldsymbol{J}\dot{\boldsymbol{\theta}}_{C} = {}^{C}\mathbb{B}_{c}^{T\,C}\mathcal{V}_{C}^{l} \in \Re^{c}. \tag{6.10} $$

Here ${}^{C}\mathbb{B}_{c}^{T}(\boldsymbol{q}_{C})^{C}\mathcal{V}_{C}^{l}$ represents a vector of restricted velocities at the contact points.

Let ${}^{D_k}\mathcal{F}_{D_k}^{l}$ be the forces and moments (wrenches) applied to the object at contact point $\mathcal{X}_{D_k}$ by the jth finger with respect to $\{D_k\}$; $\mathcal{F}_O$ is the net object wrench at O_O with respect to $\{W\}$, resulting from the finger wrenches. Note that the wrenches applied by the fingers are restricted by the contact types given in (3.15).

The wrenches applied to each contact point by the fingers are stacked as follows:

$$ {}^{C}\mathcal{F}_{C}^{l} = \begin{bmatrix} {}^{D_1}\mathcal{F}_{D_1}^{l} \\ \vdots \\ {}^{D_p}\mathcal{F}_{D_p}^{l} \end{bmatrix}. $$

The instantaneous power defined in the object coordinate frame and the one defined in the contact coordinate frame must be the same. Therefore, using (6.10), the following relationship is obtained:

$$ \begin{aligned} \mathcal{V}_{O}^{T}\mathcal{F}_{O} &= \left({}^{C}\mathbb{B}_{c}^{T\,C}\mathcal{V}_{C}^{l}\right)^{T}\left({}^{C}\mathbb{B}_{c}^{T\,C}\mathcal{F}_{C}^{l}\right) \\ &= \left({}^{C}\boldsymbol{G}^{T}\mathcal{V}_{O}\right)^{T}\left({}^{C}\mathbb{B}_{c}^{T\,C}\mathcal{F}_{C}^{l}\right) \\ &= \mathcal{V}_{O}^{T\,C}\boldsymbol{G}\left({}^{C}\mathbb{B}_{c}^{T\,C}\mathcal{F}_{C}^{l}\right). \end{aligned} \tag{6.11} $$

From (6.11), the force generated at O_O with respect to $\{W\}$ is given as follows:

$$ \mathcal{F}_{O} = {}^{C}\boldsymbol{G}\left({}^{C}\mathbb{B}_{c}^{T\,C}\mathcal{F}_{C}^{l}\right). \tag{6.12} $$

6.2.3 Constraint Types

Various grasp types are illustrated in Fig. 6.3. In the case of Fig. 6.3A, if the constraint points are locked, the object cannot move even infinitesimally. Such a grasp type is referred to as the *form closure* (more precisely the *first-order form closure*). A form-closed grasp is also referred to as the *power grasp* or *enveloping grasp*. In the case of Fig. 6.3B, the object cannot move much but can infinitesimally rotate around the barycenter even if the constraint points are locked, because the contact points do not constrain the object in the tangential directions. This grasp type is a *form closure* of higher order. The order of the *form closure* depends on the curvature of the contact surface of the object or the hand. It is easily understood that the object can rotate around the barycenter in the case of Fig. 6.3C, even if the constraint points are locked. However, if the friction forces are considered, the grasp illustrated in Fig. 6.3C can keep the balance. Hence such a grasp is characterized as a *force closure*. Note that all the form-closure grasps are also force closure.

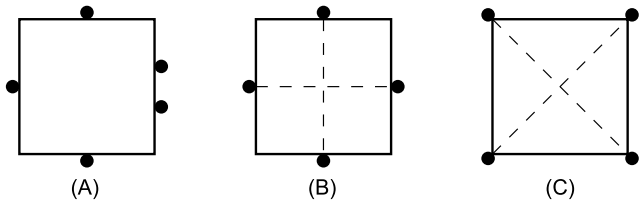

FIGURE 6.3 Various grasp types. The square denotes the grasped object. The ● symbols are the grasping points. (A) First order form-closure. (B) Second order form-closure. (C) Non-form-closure.

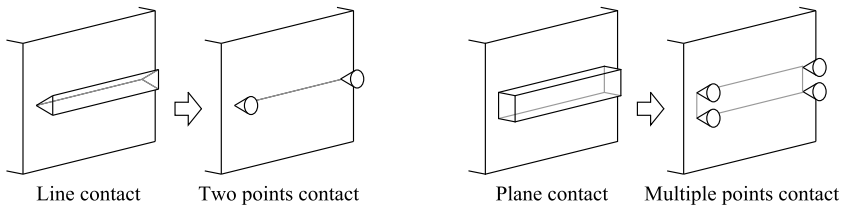

FIGURE 6.4 Approximation of a line contact and a plane contact.

In order to analyze the constraints imposed by the fingers, the line contacts and the plane contacts will be replaced by corresponding multipoint contacts, as illustrated in Fig. 6.4. Let ψ_j be the gap between the object and the jth fingertip; ψ_j will be a function of the object's position and orientation, $\mathcal{X}_O$, and the joint coordinates of the jth finger, $\boldsymbol{\theta}_{D_k}$. If ψ_j is negative, the jth fingertip penetrates into the object. If penetration of a fingertip into the object is not permitted, inequality constraint conditions have to be defined at each contact point, as follows:

$$\psi_j\left(\mathcal{X}_O, \boldsymbol{\theta}_{D_k}\right) \geq 0. \tag{6.13}$$

6.2.4 Form Closure

There are several definitions for form closure. In [2], form closure was defined as

A set of contact constraints is defined as the form closure if, for all object motions, at least one contact constraint is violated.

Reference [24] defined the form closure using the gap function given in (6.13). Suppose the following equation holds for $\mathcal{X}_O$ and $\boldsymbol{\theta}_{D_k}$:

$$\psi_j\left(\mathcal{X}_O, \boldsymbol{\theta}_{D_k}\right) = 0 \quad \forall j = 1, ..., c, \tag{6.14}$$

where c is the number of constraints. The definition of the form closure in [24] is

A grasp $(\mathcal{X}_O, \boldsymbol{\theta}_{D_k})$ has a form closure if and only if the following implication holds:

$$\boldsymbol{\psi}\left(\mathcal{X}_O + d\mathcal{X}_O, \boldsymbol{\theta}_{D_k}\right) \geq \mathbf{0} \quad \Rightarrow \quad d\mathcal{X}_O = \mathbf{0} \tag{6.15}$$

where $\boldsymbol{\psi}$ is the c-dimensional vector of gap functions with jth component equal to $\psi_j\left(\mathcal{X}_O, \boldsymbol{\theta}_{D_k}\right)$.

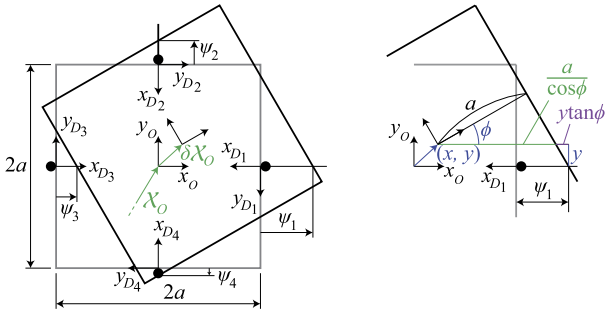

FIGURE 6.5 Constraint analysis. The 6D object position/orientation $\mathcal{X}_O$ moves to $\mathcal{X}_O + \delta\mathcal{X}_O$, and the finger tips do not move.

If the first-order approximation of $\boldsymbol{\psi}\left(\mathcal{X}_O + d\mathcal{X}_O, \boldsymbol{\theta}_{D_k}\right)$ is considered, the definition of the form closure (6.15) can be written as

$$\boldsymbol{\psi}\left(\mathcal{X}_O + d\mathcal{X}_O, \boldsymbol{\theta}_{D_k}\right) \simeq \frac{\partial \boldsymbol{\psi}\left(\mathcal{X}_O, \boldsymbol{\theta}_{D_k}\right)}{\partial \mathcal{X}_O} d\mathcal{X}_O \geq \mathbf{0} \quad \Rightarrow \quad d\mathcal{X}_O = \mathbf{0}. \tag{6.16}$$

If a grasp satisfies (6.16), the grasp is *first-order form-closed*.

Case Study

Using the planar case illustrated in Fig. 6.3B, the form closure is analyzed as a case study. Suppose a square object is constrained at $(x, y) = (a, 0)$, $(0, a)$, $(-a, 0)$, and $(0, -a)$. The initial position and orientation of the object is $(x_0, y_0, \phi_0) = (0, 0, 0)$. When the object moves to (x, y, ϕ), some constraints may be violated and some constraints may break as illustrated in Fig. 6.5, if the constraint points are locked. Gap functions ψ_j are defined as gaps between the constraint position and the edge of the object along the x_{D_k}-axes.

As illustrated in Fig. 6.5, point $(a, -y_0, 0)$ on the right edge of the object moves to $(a - \psi_1, 0, \phi)$ when the object moves from $(0, 0, 0)$ to (x, y, ϕ). This transformation is given as

$$\begin{bmatrix} a - \psi_1 \\ 0 \end{bmatrix} = \begin{bmatrix} \cos\phi & -\sin\phi \\ \sin\phi & \cos\phi \end{bmatrix} \begin{bmatrix} a \\ -y_a \end{bmatrix} + \begin{bmatrix} x \\ y \end{bmatrix}. \tag{6.17}$$

By eliminating y_a from (6.17), the gap function ψ_1 is obtained. In the same manner, ψ_j for $j = 2, 3, 4$ are obtained. Finally, the constraint condition is given as

$$\begin{bmatrix} \psi_1(x, y, \phi) \\ \psi_2(x, y, \phi) \\ \psi_3(x, y, \phi) \\ \psi_4(x, y, \phi) \end{bmatrix} = \begin{bmatrix} -x - y\tan\phi - \dfrac{a}{\cos\phi} + a \\ x\tan\phi - y - \dfrac{a}{\cos\phi} + a \\ x + y\tan\phi - \dfrac{a}{\cos\phi} + a \\ -x\tan\phi + y - \dfrac{a}{\cos\phi} + a \end{bmatrix} \geq \begin{bmatrix} 0 \\ 0 \\ 0 \\ 0 \end{bmatrix}. \tag{6.18}$$

It is obvious that $\psi_j(0,0,0)=0$ for $j=1,...,4$. The first-order approximation of (6.18) around $\psi_j(x,y,\phi)=(0,0,0)$ is

$$\begin{bmatrix}\psi_1(\delta x,\delta y,\delta\psi)\\ \psi_2(\delta x,\delta y,\delta\psi)\\ \psi_3(\delta x,\delta y,\delta\psi)\\ \psi_4(\delta x,\delta y,\delta\psi)\end{bmatrix} \simeq \boldsymbol{\psi}(0,0,0)+\left\{\frac{\partial\boldsymbol{\psi}}{\partial x}\delta x+\frac{\partial\boldsymbol{\psi}}{\partial y}\delta y+\frac{\partial\boldsymbol{\psi}}{\partial\phi}\delta\phi\right\}\Big|_{(0,0,0)} = \begin{bmatrix}-\delta x\\ -\delta y\\ \delta x\\ \delta y\end{bmatrix} \geq \begin{bmatrix}0\\0\\0\\0\end{bmatrix}. \quad (6.19)$$

The solutions to (6.19) include $(\delta x,\delta y,\delta\phi)=(0,0,\delta\phi)$. Since the grasp illustrated in Fig. 6.3B allows for infinitesimal rotations $\delta\phi$, it follows that the grasp cannot be first-order form-closed.

The second-order approximation of (6.18) around $\psi_j(x,y,\phi)=(0,0,0)$ becomes as follows:

$$\begin{bmatrix}\psi_1(\delta x,\delta y,\delta\psi)\\ \psi_2(\delta x,\delta y,\delta\psi)\\ \psi_3(\delta x,\delta y,\delta\psi)\\ \psi_4(\delta x,\delta y,\delta\psi)\end{bmatrix} \simeq \begin{bmatrix}-\delta x-\delta y\delta\phi-\frac{a}{2}(\delta\phi)^2\\ -\delta y+\delta x\delta\phi-\frac{a}{2}(\delta\phi)^2\\ \delta x+\delta y\delta\phi-\frac{a}{2}(\delta\phi)^2\\ \delta y-\delta x\delta\phi-\frac{a}{2}(\delta\phi)^2\end{bmatrix} \geq \begin{bmatrix}0\\0\\0\\0\end{bmatrix}. \quad (6.20)$$

The only solution to (6.20) is $(\delta x,\delta y,\delta\phi)=(0,0,0)$. Therefore, the grasp illustrated in Fig. 6.3B is second-order form-closed.

6.2.5 Force Closure

In Section 6.2.4, frictionless constraints were assumed. However, because of friction forces, a grasp may be maintained for all object motions even if the grasp is not form-closed. Such grasps are referred to as the *force closure* or *force-closed*. The main difference between a *form closure* and a *force closure* is the consideration of the friction at the grasping points.

Contact joints with friction were discussed in Section 2.9.3. The cases of point contact with friction and a soft-finger contact were formulated in (3.9) and (3.11), respectively. A box grasped by two fingers and the respective friction cones are illustrated in Fig. 6.6. The half-angle of the friction cone is given by $\tan^{-1}\mu$, $\mu>0$ being the static friction coefficient (cf. Section 2.9.3).

Definition of Force Closure

The definition of *force closure*, according to [16], is as follows:

A grasp is a force closure if, [for] any given external wrench $\mathcal{F}_e$ ($\mathcal{F}_e\in\Re^6$ in 3D grasping, while $\mathcal{F}_e\in\Re^3$ in 2D grasping) applied to the object, there exist contact forces $({}^C\mathbb{B}_c^T\ {}^C\mathcal{F}_C^l)\in FC$ such that

$${}^C\boldsymbol{G}\left({}^C\mathbb{B}_c^T\ {}^C\mathcal{F}_C^l\right)=-\mathcal{F}_e. \quad (6.21)$$

Here FC is a set of forces within the friction cones defined as $FC=\left\{f_{D_k}\in FC_{D_k};\ j=1,\cdots,p\right\}$. See (3.9) and (3.11) for FC_{D_k}. The l.h.s. of (6.21) is equivalent to $\mathcal{F}_O$ calculated in (6.12).

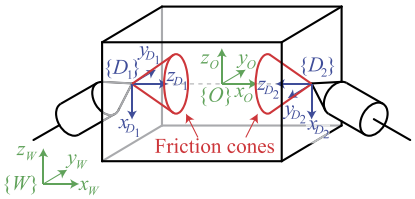

FIGURE 6.6 Friction cones when two soft fingers grasp a box.

Case Study

Suppose two soft fingers grasp a box as illustrated in Fig. 6.6 (this example is the same as Example 5.2 in [16]). It is clear that the grasp illustrated in Fig. 6.6 is not form-closed. The force closure of this example is examined in this case study.

The rotation matrices $\boldsymbol{R}_{D_1}$ and $\boldsymbol{R}_{D_1}$ are

$$\boldsymbol{R}_{D_1} = \begin{bmatrix} 0 & 0 & 1 \\ 0 & 1 & 0 \\ -1 & 0 & 0 \end{bmatrix}, \qquad \boldsymbol{R}_{D_2} = \begin{bmatrix} 0 & 0 & -1 \\ 0 & -1 & 0 \\ -1 & 0 & 0 \end{bmatrix}. \tag{6.22}$$

The position vectors $\boldsymbol{r}_{D_1}$ and $\boldsymbol{r}_{D_2}$ are given as $\boldsymbol{r}_{D_1} = \begin{bmatrix} -r & 0 & 0 \end{bmatrix}^T$ and $\boldsymbol{r}_{D_2} = \begin{bmatrix} r & 0 & 0 \end{bmatrix}^T$, respectively.

Here ${}^{D_1}\mathbb{X}$ and ${}^{D_2}\mathbb{X}$ are calculated from (6.2) as

$${}^{D_1}\mathbb{X} = \begin{bmatrix} 0 & 0 & -1 & 0 & -r & 0 \\ 0 & 1 & 0 & 0 & 0 & -r \\ 1 & 0 & 0 & 0 & 0 & 0 \\ 0 & 0 & 0 & 0 & 0 & -1 \\ 0 & 0 & 0 & 0 & 1 & 0 \\ 0 & 0 & 0 & 1 & 0 & 0 \end{bmatrix}, \qquad {}^{D_2}\mathbb{X} = \begin{bmatrix} 0 & 0 & -1 & 0 & r & 0 \\ 0 & -1 & 0 & 0 & 0 & -r \\ -1 & 0 & 0 & 0 & 0 & 0 \\ 0 & 0 & 0 & 0 & 0 & -1 \\ 0 & 0 & 0 & 0 & -1 & 0 \\ 0 & 0 & 0 & -1 & 0 & 0 \end{bmatrix}. \tag{6.23}$$

The constraint bases ${}^{D_1}\mathbb{B}_c$ and ${}^{D_2}\mathbb{B}_c$ are given as

$${}^{D_1}\mathbb{B}_c = {}^{D_2}\mathbb{B}_c = \begin{bmatrix} 1 & 0 & 0 & 0 \\ 0 & 1 & 0 & 0 \\ 0 & 0 & 1 & 0 \\ 0 & 0 & 0 & 0 \\ 0 & 0 & 0 & 0 \\ 0 & 0 & 0 & 1 \end{bmatrix}. \tag{6.24}$$

The transpose of the grasp matrix can be calculated from (6.23) and (6.24) as

$$ {}^{C}\boldsymbol{G}^{T} = \begin{bmatrix} {}^{D_1}\mathbb{B}_c^{T}\,{}^{D_1}\mathbb{X} \\ {}^{D_2}\mathbb{B}_c^{T}\,{}^{D_2}\mathbb{X} \end{bmatrix} = \left[\begin{array}{cccccc} 0 & 0 & -1 & 0 & -r & 0 \\ 0 & 1 & 0 & 0 & 0 & -r \\ 1 & 0 & 0 & 0 & 0 & 0 \\ 0 & 0 & 0 & 1 & 0 & 0 \\ \hline 0 & 0 & -1 & 0 & r & 0 \\ 0 & -1 & 0 & 0 & 0 & -r \\ -1 & 0 & 0 & 0 & 0 & 0 \\ 0 & 0 & 0 & -1 & 0 & 0 \end{array}\right]. \tag{6.25} $$

The l.h.s. of (6.21) becomes

$$ {}^{C}\boldsymbol{G}\left({}^{C}\mathbb{B}_c^{T}\,{}^{C}\mathcal{F}_C^{l}\right) = {}^{C}\boldsymbol{G}\begin{bmatrix} {}^{D_1}\overline{\mathcal{F}}_{D_1} \\ {}^{D_2}\overline{\mathcal{F}}_{D_2} \end{bmatrix} = {}^{C}\boldsymbol{G}\left[\begin{array}{c} {}^{D_1}f_{D_{1x}} \\ {}^{D_1}f_{D_{1y}} \\ {}^{D_1}f_{D_{1z}} \\ {}^{D_1}m_{D_{1z}} \\ \hline {}^{D_2}f_{D_{2x}} \\ {}^{D_2}f_{D_{2y}} \\ {}^{D_2}f_{D_{2z}} \\ {}^{D_2}m_{D_{2z}} \end{array}\right] = \begin{bmatrix} {}^{D_1}f_{D_{1z}} - {}^{D_2}f_{D_{2z}} \\ {}^{D_1}f_{D_{1y}} - {}^{D_2}f_{D_{2y}} \\ -{}^{D_1}f_{D_{1x}} - {}^{D_2}f_{D_{2x}} \\ {}^{D_1}m_{D_{1z}} - {}^{D_2}m_{D_{2z}} \\ -r\left({}^{D_1}f_{D_{1x}} - {}^{D_2}f_{D_{2x}}\right) \\ -r\left({}^{D_1}f_{D_{1y}} + {}^{D_2}f_{D_{2y}}\right) \end{bmatrix}. \tag{6.26} $$

Therefore, if contact forces ${}^{D_1}\overline{\mathcal{F}}_{D_1} \in FC_{D_1}$ and ${}^{D_2}\overline{\mathcal{F}}_{D_2} \in FC_{D_2}$ exist for a given external wrench $\mathcal{F}_e$, such that

$$ {}^{C}\boldsymbol{G}\begin{bmatrix} {}^{D_1}\overline{\mathcal{F}}_{D_1} \\ {}^{D_2}\overline{\mathcal{F}}_{D_2} \end{bmatrix} = -\mathcal{F}_e, \tag{6.27} $$

the grasp is force-closed (but not form-closed). The friction cones, given in (3.11), are rewritten here as

$$ \left\{ FC_{D_1} : \sqrt{{}^{D_1}f_{D_{1x}}^2 + {}^{D_1}f_{D_{1y}}^2} \le \mu\ {}^{D_1}f_{D_{1z}},\ {}^{D_1}f_{D_{1z}} \ge 0,\ |{}^{D_1}m_{D_{1z}}| \le \gamma\ {}^{D_1}f_{D_{1z}} \right\}, $$
$$ \left\{ FC_{D_2} : \sqrt{{}^{D_2}f_{D_{2x}}^2 + {}^{D_2}f_{D_{2y}}^2} \le \mu\ {}^{D_2}f_{D_{2z}},\ {}^{D_2}f_{D_{2z}} \ge 0,\ |{}^{D_2}m_{D_{2z}}| \le \gamma\ {}^{D_2}f_{D_{2z}} \right\}. $$

If point contacts with friction are assumed instead of soft-finger contacts, as in the above case, the rotation of the object around z_{D_k} will be unconstrained. In this case, constant bases ${}^{D_1}\boldsymbol{C}_{D_1}$ and ${}^{D_2}\boldsymbol{C}_{D_2}$ are given as

$$ {}^{D_1}\mathbb{B}_c = {}^{D_2}\mathbb{B}_c = \begin{bmatrix} 1 & 0 & 0 \\ 0 & 1 & 0 \\ 0 & 0 & 1 \\ 0 & 0 & 0 \\ 0 & 0 & 0 \\ 0 & 0 & 0 \end{bmatrix}. \tag{6.28} $$

The transpose of the grasp matrix, obtained from (6.23) and (6.28), can be calculated as

$$ {}^{C}\boldsymbol{G}^{T} = \begin{bmatrix} {}^{D_1}\mathbb{B}_c^{T\,D_1}\mathbb{X} \\ {}^{D_2}\mathbb{B}_c^{T\,D_2}\mathbb{X} \end{bmatrix} = \left[\begin{array}{cccccc} 0 & 0 & -1 & 0 & -r & 0 \\ 0 & 1 & 0 & 0 & 0 & -r \\ 1 & 0 & 0 & 0 & 0 & 0 \\ \hline 0 & 0 & -1 & 0 & r & 0 \\ 0 & -1 & 0 & 0 & 0 & -r \\ -1 & 0 & 0 & 0 & 0 & 0 \end{array}\right]. \tag{6.29} $$

The l.h.s. of (6.21) becomes

$$ {}^{C}\boldsymbol{G}\left({}^{C}\mathbb{B}_c^{T\,C}\mathcal{F}_C^{l}\right) = {}^{C}\boldsymbol{G}\begin{bmatrix} {}^{D_1}\overline{\mathcal{F}}_{D_1} \\ \hline {}^{D_2}\overline{\mathcal{F}}_{D_2} \end{bmatrix} = {}^{C}\boldsymbol{G}\left[\begin{array}{c} {}^{D_1}f_{D_{1x}} \\ {}^{D_1}f_{D_{1y}} \\ {}^{D_1}f_{D_{1z}} \\ \hline {}^{D_2}f_{D_{2x}} \\ {}^{D_2}f_{D_{2y}} \\ {}^{D_2}f_{D_{2z}} \end{array}\right] = \begin{bmatrix} {}^{D_1}f_{D_{1z}} - {}^{D_2}f_{D_{2z}} \\ {}^{D_1}f_{D_{1y}} - {}^{D_2}f_{D_{2y}} \\ -{}^{D_1}f_{D_{1x}} - {}^{D_2}f_{D_{2x}} \\ 0 \\ -r\left({}^{D_1}f_{D_{1x}} - {}^{D_2}f_{D_{2x}}\right) \\ -r\left({}^{D_1}f_{D_{1y}} + {}^{D_2}f_{D_{2y}}\right) \end{bmatrix}. \tag{6.30} $$

It is clear from (6.30) that the external moment around x_O cannot be controlled, neither by ${}^{D_1}\overline{\mathcal{F}}_{D_1}$ nor by ${}^{D_2}\overline{\mathcal{F}}_{D_2}$.

From the above discussion it should be apparent that the grasp illustrated in Fig. 6.6 is not force-closed, when the contact model is a point contact with friction (cf. (3.9)). On the other hand, when a soft-finger contact model is assumed, the grasp will be force-closed. It should be also obvious that, if a contact model without friction is assumed, the grasp cannot be force-closed.

6.3 MULTIARM OBJECT MANIPULATION CONTROL METHODS

6.3.1 Background of Multiarm Object Manipulation

In order to achieve an object manipulation with a dual-arm manipulator system without applying an excessive force to the object, the master-slave control approach was proposed in the pioneering work [17]. According to the approach, one of the robot arms behaves as a master and controls the position of the object, while the other arm behaves as a slave and controls the internal wrenches imposed on the object. Other control approaches for cooperating manipulators, studied throughout the years, are the hybrid position/force [5,33,27,18] and the impedance [22,26,19,3,6,14] control methods.

With the focus on internal wrench control, virtual constructs have been introduced such as the *virtual linkage* [28] and the *virtual sticks* [27].

Another related field of research is the cooperative object transportation by multiple mobile robots. In this field, the leader-follower-type control schemes have been studied enthusiastically [13,7]. The leader-follower-type control between two humanoid robots was

discussed in [30]. Studies on cooperation between a humanoid robot and a human have also been carried out [32,1]. Symmetry (i.e. not leader-follower)-type cooperation among multiple humanoid robots was proposed in [29,31].

6.3.2 Kinematics and Statics of Multiarm Cooperation

Let $(\boldsymbol{r}, \boldsymbol{R})$ denote the 6D position of a rigid body. A *small displacement* of the body in 6D can be expressed as $(\delta\boldsymbol{r}, \delta\boldsymbol{R})$, where

$$\delta\boldsymbol{r} = \boldsymbol{r}' - \boldsymbol{r}, \tag{6.31}$$

$$\delta\boldsymbol{R} = \boldsymbol{R}'\boldsymbol{R}^T. \tag{6.32}$$

Here $(\boldsymbol{r}', \boldsymbol{R}')$ is the 6D position of the body after the displacement. The angular part of the displacement can also be expressed by a vector as follows:

$$\delta\boldsymbol{\phi} = (\ln\ \delta\boldsymbol{R})^\vee, \tag{6.33}$$

where $(\ln\ \delta\boldsymbol{R}) = [\delta\boldsymbol{\phi}^\times]$ [8]. The $()^\vee$ operator extracts a vector from a skew-symmetric matrix, i.e.

$$\left[\delta\boldsymbol{\phi}^\times\right]^\vee = \begin{bmatrix} 0 & -\delta\phi_z & \delta\phi_y \\ \delta\phi_z & 0 & -\delta\phi_x \\ -\delta\phi_y & \delta\phi_x & 0 \end{bmatrix}^\vee \equiv \begin{bmatrix} \delta\phi_x \\ \delta\phi_y \\ \delta\phi_z \end{bmatrix}. \tag{6.34}$$

The angular displacement vector $\delta\boldsymbol{\phi}$ can then be obtained as [8,16]

$$\delta\boldsymbol{\phi} = (\ln\ \delta\boldsymbol{R})^\vee = \begin{cases} \boldsymbol{0} & \text{if } \delta\boldsymbol{R} = \boldsymbol{E}_3 \\ |\delta\phi|\dfrac{\boldsymbol{t}}{\|\boldsymbol{t}\|} & \text{otherwise,} \end{cases} \tag{6.35}$$

where

$$\delta\boldsymbol{R} = \begin{bmatrix} r_{11} & r_{12} & r_{13} \\ r_{21} & r_{22} & r_{23} \\ r_{31} & r_{32} & r_{33} \end{bmatrix}, \quad \boldsymbol{t} = \begin{bmatrix} r_{32} - r_{23} \\ r_{13} - r_{31} \\ r_{21} - r_{12} \end{bmatrix}, \quad |\delta\phi| = \text{atan2}\left(\|\boldsymbol{t}\|, r_{11} + r_{22} + r_{33} - 1\right).$$

Note that $\delta\phi$ is defined here in $-\pi < \delta\phi < \pi$, and $\boldsymbol{t}$ includes the sign of $\delta\phi$. Using the above notation, in what follows the small displacement of the rigid body in 6D will be expressed as

$$\delta\mathcal{X} \equiv \begin{bmatrix} \delta\boldsymbol{r} \\ \delta\boldsymbol{\phi} \end{bmatrix}. \tag{6.36}$$

Suppose p robot arms grasp an object, as illustrated in Fig. 6.7. As clarified in Section 6.1, it is assumed that the robot hands grasp the object firmly whereby each hand impresses a

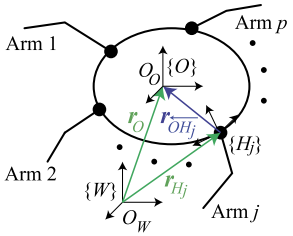

FIGURE 6.7 p robot arms that grasp an object.

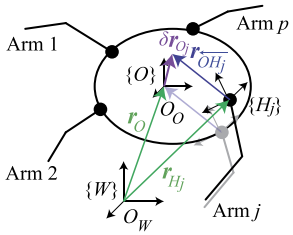

FIGURE 6.8 Virtual displacement at the tip of the virtual stick.

wrench bilaterally. Let $\{O\}$ and $\{H_j\}$ be coordinate frames fixed on the object and at the hand of Arm j, respectively, and $\{W\}$ be the inertial coordinate frame; O_O and O_W denote the origins of the coordinate frames $\{O\}$ and $\{W\}$.

Furthermore, let $(\boldsymbol{r}_{H_j}, \boldsymbol{R}_{H_j})$ and $(\boldsymbol{r}_O, \boldsymbol{R}_O)$ denote the 6D position of Arm j at the grasping point and of the grasped object, respectively. Vector ${}^{H_j}\boldsymbol{r}_{\overleftarrow{OH_j}}$ is the 3D vector pointing from grasping point $\boldsymbol{r}_{H_j}$ to O_O, w.r.t. the hand coordinate frame $\{H_j\}$. When the grasped object is rigid and does not deform (as assumed here), the vector ${}^{H_j}\boldsymbol{r}_{\overleftarrow{OH_j}}$ will be constant in coordinate frame $\{H_j\}$. Vector ${}^{H_j}\boldsymbol{r}_{\overleftarrow{OH_j}}$ is represented as $\boldsymbol{r}_{\overleftarrow{OH_j}} = \boldsymbol{R}_{H_j}{}^{H_j}\boldsymbol{r}_{\overleftarrow{OH_j}}$ in the inertial coordinate frame $\{W\}$. Note that ${}^{H_j}\boldsymbol{r}_{\overleftarrow{OH_j}}$ can be considered a stick fixed in the coordinate frame $\{H_j\}$. This vector was named the *virtual stick* in [27].

The position of the tip and the orientation of $\boldsymbol{r}_{\overleftarrow{OH_j}}$ are represented by $\boldsymbol{r}_{O_j}$ $(= \boldsymbol{r}_{H_j} + \boldsymbol{r}_{\overleftarrow{OH_j}})$ and $\boldsymbol{R}_{O_j}$, respectively. Since ${}^{H_j}\boldsymbol{r}_{\overleftarrow{OH_j}}$ is constant in coordinate frame $\{H_j\}$, $\boldsymbol{r}_{O_j}$ is equal to $\boldsymbol{r}_O$, and $\boldsymbol{R}_{O_j}$ is equal to $\boldsymbol{R}_O$. However, if a virtual displacement is considered, $\boldsymbol{r}_{O_j}$ and $\boldsymbol{R}_{O_j}$ will not always be equal to $\boldsymbol{r}_O$ and $\boldsymbol{R}_O$, respectively (see Fig. 6.8).

Let $\boldsymbol{q}_j$ be the joint angle vector of Arm j. A small displacement of the hand of Arm j can be expressed as

$$\delta\mathcal{X}_{O_j} = \begin{bmatrix} \delta\boldsymbol{r}_{O_j} \\ \delta\boldsymbol{\phi}_{O_j} \end{bmatrix} = \boldsymbol{J}_{O_j}\delta\boldsymbol{q}_j, \tag{6.37}$$

where $\boldsymbol{J}_{O_j}$ is the Jacobian matrix of Arm j.

6.3.3 Force and Moment Applied to the Object

Let ${}^{H_j}\mathcal{F}_{H_j}$ and $\mathcal{F}_{O_j}$ be the wrenches applied to the grasped object by Arm j at $\mathcal{X}_{H_j}$ with respect to $\{H_j\}$ and at O_O with respect to $\{W\}$, accordingly. The relationship between ${}^{H_j}\mathcal{F}_{H_j}$ and $\mathcal{F}_{O_j}$ is given as

$$\mathcal{F}_{O_j} = {}^{O}\mathbb{X}_{H_j}^{T}\,{}^{H_j}\mathcal{F}_{H_j}, \tag{6.38}$$

where ${}^{O}\mathbb{X}_{H_j}^{T}$ is the wrench transform matrix from $\{H_j\}$ to $\{O\}$ given in (2.7). The wrench ${}^{H_j}\mathcal{F}_{H_j}$ is calculated from the possible force ${}^{H_j}\overline{\mathcal{F}}_{H_j} \in \Re^{6\times c_j}$ (cf. (3.15)) as

$${}^{H_j}\mathcal{F}_{H_j} = {}^{H_j}\mathbb{B}_c\,{}^{H_j}\overline{\mathcal{F}}_{H_j}. \tag{6.39}$$

Here ${}^{H_j}\mathbb{B}_c$ is the constraint basis at the contact point with respect to $\{H_j\}$ (see Section 2.9.3). Since the robot hands firmly grasp the object, ${}^{H_j}\mathbb{B}_c$ becomes a 6D identity matrix (${}^{H_j}\mathbb{B}_c = \boldsymbol{E}_6$).

When p robot arms grasp an object, the resultant wrench is given as

$$\begin{aligned}\mathcal{F}_O^A &= \sum_{j=1}^{p}\mathcal{F}_{O_j} = \boldsymbol{E}_{6\times 6p}\mathcal{F}_O, \\ \boldsymbol{E}_{6\times 6p} &\equiv \begin{bmatrix}\boldsymbol{E}_6 & \cdots & \boldsymbol{E}_6\end{bmatrix} \in \Re^{6\times 6p}, \\ \mathcal{F}_O &\equiv \begin{bmatrix}\mathcal{F}_{O_1}^T & \cdots & \mathcal{F}_{O_p}^T\end{bmatrix}^T \in \Re^{6p},\end{aligned} \tag{6.40}$$

where $\mathcal{F}_O^A$ is the wrench that affects the movement of the object. The wrench $\mathcal{F}_O$ is obtained from the (least-squares) solution of (6.40), i.e.

$$\mathcal{F}_O = \left(\boldsymbol{E}_{6\times 6p}\right)^{\#}\mathcal{F}_O^A + \boldsymbol{N}\left(\boldsymbol{E}_{6\times 6p}\right)\mathcal{F}_O^a, \tag{6.41}$$

where $\left(\boldsymbol{E}_{6\times 6p}\right)^{\#} \in \Re^{6p\times 6}$ is a generalized inverse matrix of $\boldsymbol{E}_{6\times 6p}$,

$$\boldsymbol{N}\left(\boldsymbol{E}_{6\times 6p}\right) = \boldsymbol{E}_{6p} - \left(\boldsymbol{E}_{6\times 6p}\right)^{\#}\boldsymbol{E}_{6\times 6p}$$

is a projection matrix onto the null space of $\boldsymbol{E}_{6\times 6p}$, and

$$\mathcal{F}_O^a = \begin{bmatrix}\left(\mathcal{F}_{O_1}^a\right)^T & \cdots & \left(\mathcal{F}_{O_p}^a\right)^T\end{bmatrix}^T \in \Re^{6p}$$

is an arbitrary wrench.

The reduced-form representation of (6.41) can be written as

$$\begin{aligned}\mathcal{F}_O &= \left(\boldsymbol{E}_{6\times 6p}\right)^{\#}\mathcal{F}_O^A + \boldsymbol{V}\mathcal{F}_O^I = \boldsymbol{U}\mathcal{F}_O^{AI}, \\ \boldsymbol{U} &\equiv \begin{bmatrix}\left(\boldsymbol{E}_{6\times 6p}\right)^{\#} & \boldsymbol{V}\end{bmatrix} \in \Re^{6p\times 6p}, \\ \mathcal{F}_O^{AI} &\equiv \begin{bmatrix}\mathcal{F}_O^A \\ \mathcal{F}_O^I\end{bmatrix} \in \Re^{6p},\end{aligned} \tag{6.42}$$

where $\boldsymbol{V} \in \Re^{6p \times 6(p-1)}$ is a matrix that satisfies

$$\boldsymbol{E}_{6\times 6p}\boldsymbol{V} = \boldsymbol{0}_{6\times 6(p-1)}, \tag{6.43}$$

and $\boldsymbol{0}_{6\times 6(p-1)}$ is the $6 \times 6(p-1)$ zero matrix; $\mathcal{F}_O^I$ is a set of wrenches defined as

$$\mathcal{F}_O^I = \left[\left(\mathcal{F}_{O_1}^I\right)^T \quad \cdots \quad \left(\mathcal{F}_{O_{p-1}}^I\right)^T\right]^T \in \Re^{6(p-1)}, \tag{6.44}$$

and $\mathcal{F}_{O_j}^I$ corresponds to the jth internal wrench. The motion of the object is unaffected by the internal wrenches by definition.

Case Study

The two expressions (6.41) and (6.42) for $\mathcal{F}_O$ are compared taking $p = 2$ as a case study. The pseudoinverse is used as a generalized inverse to compare the two expressions.

First, $\mathcal{F}_O$ is derived from (6.41) as

$$\begin{aligned}\mathcal{F}_O &= \frac{1}{2}\begin{bmatrix}\boldsymbol{E}_6\\ \boldsymbol{E}_6\end{bmatrix}\mathcal{F}_O^A + \frac{1}{2}\begin{bmatrix}\boldsymbol{E}_6 & -\boldsymbol{E}_6\\ -\boldsymbol{E}_6 & \boldsymbol{E}_6\end{bmatrix}\mathcal{F}_O^a \\ &= \frac{1}{2}\begin{bmatrix}\boldsymbol{E}_6\\ \boldsymbol{E}_6\end{bmatrix}\mathcal{F}_O^A + \frac{1}{2}\begin{bmatrix}\boldsymbol{E}_6\\ -\boldsymbol{E}_6\end{bmatrix}\mathcal{F}_{O_1}^a + \frac{1}{2}\begin{bmatrix}-\boldsymbol{E}_6\\ \boldsymbol{E}_6\end{bmatrix}\mathcal{F}_{O_2}^a,\end{aligned} \tag{6.45}$$

where $\mathcal{F}_{O_1}^a$ and $\mathcal{F}_{O_2}^a$ are arbitrary 6D wrenches. It should be apparent that the second and third terms on the r.h.s. are redundant expressions.

Next, $\mathcal{F}_O$ is derived using (6.42). The general form of matrix $\boldsymbol{V}$ that satisfies (6.43) is given as

$$\boldsymbol{V} = \xi\begin{bmatrix}\boldsymbol{E}_6\\ -\boldsymbol{E}_6\end{bmatrix}, \tag{6.46}$$

where ξ is an arbitrary scalar. Substituting (6.46) into (6.42), $\mathcal{F}_O$ becomes

$$\mathcal{F}_O = \frac{1}{2}\begin{bmatrix}\boldsymbol{E}_6\\ \boldsymbol{E}_6\end{bmatrix}\mathcal{F}_O^A + \xi\begin{bmatrix}\boldsymbol{E}_6\\ -\boldsymbol{E}_6\end{bmatrix}\mathcal{F}_O^{Ia}, \tag{6.47}$$

where $\mathcal{F}_O^{Ia}$ is an arbitrary 6D wrench.

Comparing (6.47) with (6.45), it becomes apparent that (6.42) is a reduced-form representation of (6.41). The main advantages of (6.42) are that $\boldsymbol{U}$ is a square matrix of size $6p$ and that $\boldsymbol{V}$ is specified so that $\boldsymbol{U}$ is invertible.

6.3.4 Load Distribution

Consider the following matrix:

$$\left(\boldsymbol{E}_{6\times 6p}\right)^{\#} = \begin{bmatrix} \left(1-\sum_{j=2}^{p}\lambda_j\right)\boldsymbol{E}_6 \\ \lambda_2\boldsymbol{E}_6 \\ \cdots \\ \lambda_p\boldsymbol{E}_6 \end{bmatrix}, \tag{6.48}$$

where $0 \leq \lambda_j \leq 1$ and $0 \leq \sum_{j=2}^{p}\lambda_j \leq 1$. It can be verified that the above matrix satisfies the definitive equation of a generalized inverse matrix, i.e. $\boldsymbol{E}_{6\times 6p}\left(\boldsymbol{E}_{6\times 6p}\right)^{\#}\boldsymbol{E}_{6\times 6p} = \boldsymbol{E}_{6\times 6p}$. Substituting (6.48) into (6.42), the net wrench $\mathcal{F}_O$, that should be applied at point O_O by the p robot arms, can be obtained as

$$\mathcal{F}_O = \begin{bmatrix} \mathcal{F}_{O_1} \\ \mathcal{F}_{O_2} \\ \vdots \\ \mathcal{F}_{O_p} \end{bmatrix} = \begin{bmatrix} \left(1-\sum_{j=2}^{p}\lambda_j\right)\boldsymbol{E}_6 \\ \lambda_2\boldsymbol{E}_6 \\ \cdots \\ \lambda_p\boldsymbol{E}_6 \end{bmatrix} \mathcal{F}_O^A + \boldsymbol{V}\mathcal{F}_O^I. \tag{6.49}$$

From this equation it is apparent that the applied force $\mathcal{F}_O^A$ can be distributed to the p robot arms in a desirable way, by setting the λ_js in an appropriate way. For example, a higher load can be distributed to the robot arms that have high-power actuators; λ_j is called the *load sharing coefficient* [25].

It is easily confirmed that $\mathcal{F}_O$ calculated from (6.49) satisfies (6.40). When λ_j is set as $\lambda_j = 1/p$ $(j = 1 \sim p)$, $\boldsymbol{E}_{6\times 6p}^{\#}$ becomes the pseudoinverse matrix, and the applied force $\mathcal{F}_O^A$ will be equally distributed to each robot arm.

6.3.5 Control of the External and Internal Wrenches

Suppose that p robot arms grasp an object and each arm applies a 6D wrench on the object. The p robot arms apply $6p$-dimensional wrenches on the object in total. In other words, the p robot arms can control $6p$-dimensional wrenches generated at the object. A 6D wrench out of the $6p$ wrenches is used to balance the applied wrench $\mathcal{F}_O^A$ defined in (6.40). The rest of the wrenches constitute a composite $6(p-1)$-dimensional wrench that is used to control the internal wrench $\mathcal{F}_O^I$ appearing in (6.42). From the relationship presented in (6.43) it is apparent that the term $\boldsymbol{V}\mathcal{F}_O^I$ in (6.42) exists in the null space of $\boldsymbol{E}_{6\times 6p}$. Hence, the $\boldsymbol{V}\mathcal{F}_O^I$ component will be annihilated when $\mathcal{F}_O$ is premultiplied by $\boldsymbol{E}_{6\times 6p}$, as shown in (6.40).

Suppose that p robot arms grasp an object as illustrated in Fig. 6.9. The number of two-combinations from p robot arms is given by ${}_pC_2 = p(p-1)/2$. Therefore, as illustrated in Fig. 6.9, $6 \times {}_pC_2 = 3p(p-1)$-dimensional internal wrenches can be considered, if an internal wrench is defined between each pair of robot arms.

However, as described above, only $6(p-1)$-dimensional internal wrenches can be controlled by p robot arms. If two robot arms grasp an object, p equals to two and hence $6 \times {}_pC_2 = 6(p-1) = 6$. In this case, the dimension of the internal wrenches is equal to the

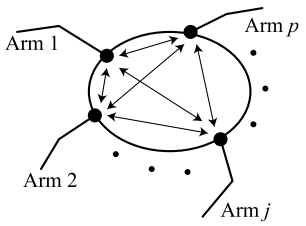

FIGURE 6.9 Internal forces defined between two-combinations from p robot arms.

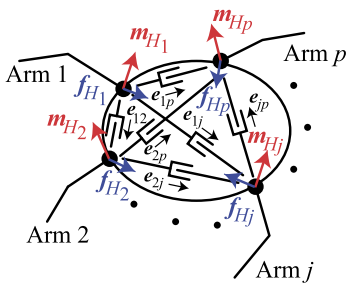

FIGURE 6.10 Concept of a virtual linkage.

controllable dimension. However, when the number of robot arms is more than two, the dimension of the internal wrenches defined for all two-combinations from p (> 2) robot arms is greater than the controllable dimension, which is expressed as $6 \times {}_pC_2 > 6(p-1)$. In such a case, $6(p-1)$-dimensional internal wrenches can be directly controlled, and the remaining $6({}_pC_2 - (p-1))$-dimensional internal wrenches are indirectly (implicitly) controlled. Hence $6(p-1)$-dimensional internal wrenches must be chosen to be directly controlled.

Virtual Linkage [28] (see also Section 3.5.2)

The virtual linkage was defined in [28] as: *"A virtual linkage associated with an n-grasp manipulation task is a $6(p-1)$-degree-of-freedom mechanism whose actuated joints characterize the object's internal forces and moments."*

Suppose p robot arms grasp an object as illustrated in Fig. 6.10. Robot Arm j applies force $\boldsymbol{f}_{H_j} \in \Re^3$ and moment $\boldsymbol{m}_{H_j} \in \Re^3$. The net wrench applied at O_O is given as

$$\mathcal{F}_O^A = \begin{bmatrix} \boldsymbol{f}_O^A \\ \boldsymbol{m}_O^A \end{bmatrix} = \begin{bmatrix} \mathbb{T}_f^T & \mathbb{T}_m^T \end{bmatrix} \begin{bmatrix} \boldsymbol{f}_H \\ \boldsymbol{m}_H \end{bmatrix}, \tag{6.50}$$

$$\mathbb{T}_f^T = \begin{bmatrix} \boldsymbol{E}_3 & \cdots & \boldsymbol{E}_3 \\ -[\boldsymbol{r}_1^\times] & \cdots & -[\boldsymbol{r}_p^\times] \end{bmatrix} \in \Re^{6\times 3p}, \quad \mathbb{T}_m^T = \begin{bmatrix} \boldsymbol{0}_3 & \cdots & \boldsymbol{0}_3 \\ \boldsymbol{E}_3 & \cdots & \boldsymbol{E}_3 \end{bmatrix} \in \Re^{6\times 3p}, \tag{6.51}$$

$$\boldsymbol{f}_H = \begin{bmatrix} \boldsymbol{f}_{H_1} \\ \vdots \\ \boldsymbol{f}_{H_p} \end{bmatrix} \in \Re^{3p}, \quad \boldsymbol{m}_H = \begin{bmatrix} \boldsymbol{m}_{H_1} \\ \vdots \\ \boldsymbol{m}_{H_p} \end{bmatrix} \in \Re^{3p}. \tag{6.52}$$

Virtual linkages are introduced between all two-combinations of the p robot arms, as illustrated in Fig. 6.10. Let $\boldsymbol{r}_{H_j}$ be the 3D position vector of the grasping point of Arm j. Note that $\boldsymbol{r}_{H_j}$ can be extracted from the first three components of $\mathcal{X}_{H_j}$.

Unit vectors $\boldsymbol{e}_{ij}$ are defined between $\boldsymbol{r}_{H_i}$ and $\boldsymbol{r}_{H_j}$ as follows:

$$\boldsymbol{e}_{ij} = \frac{\boldsymbol{r}_{H_j} - \boldsymbol{r}_{H_i}}{\|\boldsymbol{r}_{H_j} - \boldsymbol{r}_{H_i}\|}, \quad \boldsymbol{e}_{ji} = -\boldsymbol{e}_{ij}. \tag{6.53}$$

The internal force between $\boldsymbol{r}_{H_i}$ and $\boldsymbol{r}_{H_j}$ is defined as

$$\boldsymbol{f}^I_{H_{ij}} = f^{int}_{ij} \boldsymbol{e}_{ij}. \tag{6.54}$$

Here f^{int}_{ij} $(= f_{ji} \geq 0)$ is the magnitude of the internal force, whereas $\boldsymbol{e}_{ij}$ is its direction. If the magnitudes of the internal forces $\boldsymbol{f}^{int} = \begin{bmatrix} \cdots & f^{int}_{ij} & \cdots \end{bmatrix}^T \in \Re^{{}_pC_2}$ are specified, the force $\boldsymbol{f}_H$ (defined in (6.52)) that realizes the desired internal forces is given as

$$\boldsymbol{f}^I_H = \boldsymbol{V}_L \boldsymbol{f}^{int}. \tag{6.55}$$

Here $\boldsymbol{V}_L \in \Re^{3p \times {}_pC_2}$ is a matrix that relates $\boldsymbol{f}^{int} \in \Re^{{}_pC_2}$ to $\boldsymbol{f}^I_H \in \Re^{3p}$.

Using (6.50) and (6.55), the relationship between resultant/internal forces and applied wrenches is given by

$$\begin{bmatrix} \boldsymbol{f}^A_O \\ \boldsymbol{m}^A_O \\ \boldsymbol{f}^{int} \\ \boldsymbol{m}_H \end{bmatrix} = \mathbb{G} \begin{bmatrix} \boldsymbol{f}_H \\ \boldsymbol{m}_H \end{bmatrix}, \qquad \mathbb{G} = \begin{bmatrix} \mathbb{T}^T_f & \mathbb{T}^T_m \\ \boldsymbol{V}^+_L & \boldsymbol{0}_{{}_pC_2 \times 3p} \\ \boldsymbol{0}_{3p} & \boldsymbol{E}_{3p} \end{bmatrix} \in \Re^{({}_pC_2+3p+6)\times 6p}, \tag{6.56}$$

where $\boldsymbol{V}^+_L$ is the Moore–Penrose pseudoinverse matrix of $\boldsymbol{V}_L$. The matrix $\mathbb{G}$ is referred to as the *grasp description matrix* [28]. Note that the matrix $\mathbb{G}$ defined here is different from the *grasp matrix* [16] that indicates convexity conditions.

When the desired resultant wrench, the magnitudes of the internal forces, and the moments at the grasp points are given, the wrenches which should be applied to the grasp points are calculated as follows:

$$\begin{bmatrix} \boldsymbol{f}_H \\ \boldsymbol{m}_H \end{bmatrix} = \mathbb{G}^+ \begin{bmatrix} \boldsymbol{f}^A_O \\ \boldsymbol{m}^A_O \\ \boldsymbol{f}^{int} \\ \boldsymbol{m}_H \end{bmatrix}. \tag{6.57}$$

Consider as an example the case when three robot arms grasp an object, as illustrated in Fig. 6.11. The internal forces are obtained from (6.55) as follows:

$$\begin{bmatrix} \boldsymbol{f}^I_{H_1} \\ \boldsymbol{f}^I_{H_2} \\ \boldsymbol{f}^I_{H_3} \end{bmatrix} = \begin{bmatrix} \boldsymbol{e}_{12} & \boldsymbol{0}_{3\times 1} & \boldsymbol{e}_{13} \\ \boldsymbol{e}_{21} & \boldsymbol{e}_{23} & \boldsymbol{0}_{3\times 1} \\ \boldsymbol{0}_{3\times 1} & \boldsymbol{e}_{32} & \boldsymbol{e}_{31} \end{bmatrix} \begin{bmatrix} f^{int}_{12} \\ f^{int}_{23} \\ f^{int}_{31} \end{bmatrix} = \boldsymbol{V}_L \boldsymbol{f}^{int}, \tag{6.58}$$

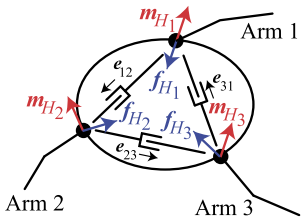

FIGURE 6.11 Three-grasp virtual linkages.

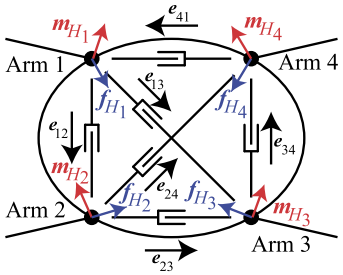

FIGURE 6.12 Four-grasp virtual linkages.

where $\boldsymbol{V}_L \in \Re^{9\times 3}$. When the three grasping points form an equilateral triangle, the unit vectors between each two grasping points are defined as follows:

$$\boldsymbol{e}_{12} = \begin{bmatrix} -\frac{1}{2} \\ -\frac{\sqrt{3}}{2} \\ 0 \end{bmatrix}, \quad \boldsymbol{e}_{23} = \begin{bmatrix} 1 \\ 0 \\ 0 \end{bmatrix}, \quad \boldsymbol{e}_{31} = \begin{bmatrix} -\frac{1}{2} \\ \frac{\sqrt{3}}{2} \\ 0 \end{bmatrix}. \tag{6.59}$$

When the unit vectors $\boldsymbol{e}_{ij}$ are determined as above, the rank of $\boldsymbol{V}_L$ is three and there is no rank deficiency.

Next, suppose that four arms grasp an object, as illustrated in Fig. 6.12. The internal forces obtained from (6.55) are

$$\begin{bmatrix} \boldsymbol{f}^I_{H_1} \\ \boldsymbol{f}^I_{H_2} \\ \boldsymbol{f}^I_{H_3} \\ \boldsymbol{f}^I_{H_4} \end{bmatrix} = \begin{bmatrix} \boldsymbol{e}_{12} & \boldsymbol{0}_{3\times 1} & \boldsymbol{0}_{3\times 1} & \boldsymbol{e}_{14} & \boldsymbol{e}_{13} & \boldsymbol{0}_{3\times 1} \\ \boldsymbol{e}_{21} & \boldsymbol{e}_{23} & \boldsymbol{0}_{3\times 1} & \boldsymbol{0}_{3\times 1} & \boldsymbol{0}_{3\times 1} & \boldsymbol{e}_{24} \\ \boldsymbol{0}_{3\times 1} & \boldsymbol{e}_{32} & \boldsymbol{e}_{34} & \boldsymbol{0}_{3\times 1} & \boldsymbol{e}_{31} & \boldsymbol{0}_{3\times 1} \\ \boldsymbol{0}_{3\times 1} & \boldsymbol{0}_{3\times 1} & \boldsymbol{e}_{43} & \boldsymbol{e}_{41} & \boldsymbol{0}_{3\times 1} & \boldsymbol{e}_{42} \end{bmatrix} \begin{bmatrix} f^{int}_{12} \\ f^{int}_{23} \\ f^{int}_{34} \\ f^{int}_{41} \\ f^{int}_{13} \\ f^{int}_{24} \end{bmatrix} = \boldsymbol{V}_L \boldsymbol{f}^{int}, \tag{6.60}$$

where $\boldsymbol{V}_L \in \Re^{12\times 6}$. When the four grasping points form a square, the unit vectors between each two grasping points are defined as follows:

$$\boldsymbol{e}_{12} = \begin{bmatrix} 0 \\ -1 \\ 0 \end{bmatrix}, \quad \boldsymbol{e}_{23} = \begin{bmatrix} 1 \\ 0 \\ 0 \end{bmatrix}, \quad \boldsymbol{e}_{34} = \begin{bmatrix} 0 \\ 1 \\ 0 \end{bmatrix}, \quad \boldsymbol{e}_{41} = \begin{bmatrix} -1 \\ 0 \\ 0 \end{bmatrix}, \quad \boldsymbol{e}_{13} = \frac{1}{\sqrt{2}} \begin{bmatrix} -1 \\ -1 \\ 0 \end{bmatrix}, \quad \boldsymbol{e}_{24} = \frac{1}{\sqrt{2}} \begin{bmatrix} 1 \\ 1 \\ 0 \end{bmatrix}. \tag{6.61}$$

When the unit vectors $\boldsymbol{e}_{ij}$ are determined as above, the rank of $\boldsymbol{V}_L$ is just five, which implies rank deficiency. In general, $\boldsymbol{V}_L$ is not always of full rank, hence $\mathbb{G}^+$ in (6.57) is not always available.

The problems of the virtual linkage model are summarized as follows:

- There are no criteria how to determine the desired magnitudes of internal forces $\boldsymbol{f}^{int}$. Note that there is no guarantee that the internal forces defined between each two pairs of grasp points will be always independent.
- In the case of dependent internal forces, the rank of grasp description matrix $\mathbb{G}$ may be deficient, as explained above (also mentioned in [28]).
- In the virtual linkage model, only the internal force along $\boldsymbol{e}_{ij}$ is controlled. Therefore, unexpected internal force/moment along other directions may be generated.

Virtual Stick [25,27]

The virtual stick model [27] can deal with 6D internal wrenches between two grasp points. When two robot arms grasp an object ($p = 2$), $\boldsymbol{V}$ is given by (6.46). By setting the arbitrary scalar as $\xi = -1$, $\boldsymbol{V}$ is obtained as [27]

$$\boldsymbol{V} = \begin{bmatrix} -\boldsymbol{E}_6 \\ \boldsymbol{E}_6 \end{bmatrix}. \tag{6.62}$$

With this matrix, the external/internal wrenches can be calculated as follows:

$$\begin{bmatrix} \mathcal{F}_O^A \\ \mathcal{F}_O^I \end{bmatrix} = \begin{bmatrix} (\boldsymbol{E}_{6\times 12})^+ & \boldsymbol{V} \end{bmatrix}^{-1} \mathcal{F}_O, \tag{6.63}$$

where $(\circ)^+$ denotes the (right) Moore–Penrose pseudoinverse matrix. Substituting (6.62) into (6.63), the internal wrench is obtained as

$$\mathcal{F}_O^I = \frac{1}{2}\left(\mathcal{F}_{O_2} - \mathcal{F}_{O_1}\right). \tag{6.64}$$

The above equation indicates that the internal wrench is defined as the difference between the forces generated by robot arms 1 and 2. This equation clearly presents the physical meaning of the internal force.

When the number of robot arms is more than two ($p > 2$), however, it is difficult to intuitively understand what the meaning of the internal wrench $\mathcal{F}_O^I$ obtained from (6.63) is. Note that this case is not discussed in [25,27].

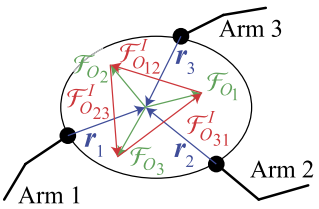

FIGURE 6.13 Internal forces generated among three robot arms.

A way of defining the internal force for the case $p > 2$ was proposed in [31]. To avoid the explicit appearance of $\boldsymbol{V}$, instead of (6.63) use

$$\begin{bmatrix} \mathcal{F}_O^A \\ \mathcal{F}_O^I \end{bmatrix} = \begin{bmatrix} \boldsymbol{E}_{6\times 6p} \\ \boldsymbol{Q} \end{bmatrix} \mathcal{F}_O . \tag{6.65}$$

The internal force can be specified via matrix $\boldsymbol{Q}$. To this end, note that matrix $\boldsymbol{U}$ in (6.42) can be obtained as

$$\boldsymbol{U} = \begin{bmatrix} \boldsymbol{E}_{6\times 6p} \\ \boldsymbol{Q} \end{bmatrix}^{-1} . \tag{6.66}$$

The method proposed in [31] is explained here through an example. Consider that three robot arms grasp an object, as illustrated in Fig. 6.13. Arm j applies the 6D wrench $\mathcal{F}_{O_j}$ to the object. The internal force between each pair of arms is not uniquely determined. However, the internal force between arms i and j can be expressed as (cf. (6.64))

$$\mathcal{F}_{O_{ij}}^I = \frac{1}{2} \left(\mathcal{F}_{O_j} - \mathcal{F}_{O_i} \right) . \tag{6.67}$$

Note that the above equation can also be derived from (6.63) with an appropriate matrix $\boldsymbol{V}$ that satisfies (6.43). Note that $\mathcal{F}_{O_{ij}}^I$, defined in (6.67), is an internal force. Furthermore, note that the sum of all $\mathcal{F}_{O_{ij}}^I$ is also an internal force, s.t. $\mathcal{F}_O^A$ will be unaffected by this force. In [31], the internal forces were defined as appropriate combinations of $\mathcal{F}_{O_{ij}}^I$.

Cooperation Among Three Robot Arms

In the case of cooperation among three robot arms, the number of two-combinations is ${}_3C_2 = 3(3-1)/2 = 3$. This means that three internal wrenches can be defined. They are denoted as $\mathcal{F}_{O_{12}}^I$, $\mathcal{F}_{O_{23}}^I$, and $\mathcal{F}_{O_{31}}^I$ (see Fig. 6.13). Note, however, that the DoFs available to control the internal wrenches are just $6(p-1) = 6(3-1) = 12$. This means that only two out of the three internal wrenches can be explicitly controlled. In other words, only two of the internal wrenches are independent. The third internal wrench can be expressed as a sum of the other two, i.e. $\mathcal{F}_{O_{31}}^I = -(\mathcal{F}_{O_{12}}^I + \mathcal{F}_{O_{23}}^I)$.

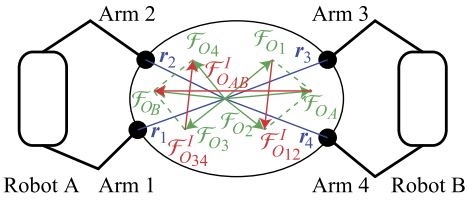

FIGURE 6.14 Cooperation between two dual-arm robots.

Suppose that $\mathcal{F}_{O_{12}}^I$ and $\mathcal{F}_{O_{23}}^I$ are chosen as the internal wrenches for explicit control; $\mathcal{F}_O^I$ can then be obtained as follows:

$$\mathcal{F}_O^I = \begin{bmatrix} \mathcal{F}_{O_{12}}^I \\ \mathcal{F}_{O_{23}}^I \end{bmatrix} = \boldsymbol{Q} \begin{bmatrix} \mathcal{F}_{O_1} \\ \mathcal{F}_{O_2} \\ \mathcal{F}_{O_3} \end{bmatrix}, \tag{6.68}$$

$$\boldsymbol{Q} = \frac{1}{2} \begin{bmatrix} -\boldsymbol{E}_6 & \boldsymbol{E}_6 & \boldsymbol{0}_6 \\ \boldsymbol{0}_6 & -\boldsymbol{E}_6 & \boldsymbol{E}_6 \end{bmatrix}.$$

Substituting (6.40) and (6.68) into (6.65), the following equation is obtained:

$$\begin{bmatrix} \mathcal{F}_O^A \\ \mathcal{F}_{O_{12}}^I \\ \mathcal{F}_{O_{23}}^I \end{bmatrix} = \begin{bmatrix} \boldsymbol{E}_{6\times 6p} \\ \boldsymbol{Q} \end{bmatrix} \begin{bmatrix} \mathcal{F}_{O_1} \\ \mathcal{F}_{O_2} \\ \mathcal{F}_{O_3} \end{bmatrix} = \begin{bmatrix} \boldsymbol{E}_6 & \boldsymbol{E}_6 & \boldsymbol{E}_6 \\ -\frac{1}{2}\boldsymbol{E}_6 & \frac{1}{2}\boldsymbol{E}_6 & \boldsymbol{0}_6 \\ \boldsymbol{0}_6 & -\frac{1}{2}\boldsymbol{E}_6 & \frac{1}{2}\boldsymbol{E}_6 \end{bmatrix} \begin{bmatrix} \mathcal{F}_{O_1} \\ \mathcal{F}_{O_2} \\ \mathcal{F}_{O_3} \end{bmatrix}. \tag{6.69}$$

Grasp wrenches $\mathcal{F}_{O_j}$, that can be used to achieve the desired $\mathcal{F}^A$, $\mathcal{F}_{O_{12}}^I$, and $\mathcal{F}_{O_{23}}^I$, are calculated as follows:

$$\begin{bmatrix} \mathcal{F}_{O_1} \\ \mathcal{F}_{O_2} \\ \mathcal{F}_{O_3} \end{bmatrix} = \begin{bmatrix} \boldsymbol{E}_{6\times 6p} \\ \boldsymbol{Q} \end{bmatrix}^{-1} \begin{bmatrix} \mathcal{F}_O^A \\ \mathcal{F}_{O_{12}}^I \\ \mathcal{F}_{O_{23}}^I \end{bmatrix} = \frac{1}{3} \begin{bmatrix} \boldsymbol{E}_6 & -4\boldsymbol{E}_6 & -2\boldsymbol{E}_6 \\ \boldsymbol{E}_6 & 2\boldsymbol{E}_6 & -2\boldsymbol{E}_6 \\ \boldsymbol{E}_6 & 2\boldsymbol{E}_6 & 4\boldsymbol{E}_6 \end{bmatrix} \begin{bmatrix} \mathcal{F}_O^A \\ \mathcal{F}_{O_{12}}^I \\ \mathcal{F}_{O_{23}}^I \end{bmatrix} = \begin{bmatrix} \boldsymbol{E}_{6\times 6p}^+ & \boldsymbol{V} \end{bmatrix} \begin{bmatrix} \mathcal{F}_O^A \\ \mathcal{F}_O^I \end{bmatrix}, \tag{6.70}$$

$$\mathcal{F}_O^I = \begin{bmatrix} \mathcal{F}_{O_{12}}^I \\ \mathcal{F}_{O_{23}}^I \end{bmatrix}, \quad \boldsymbol{E}_{6\times 6p}^+ = \frac{1}{3} \begin{bmatrix} \boldsymbol{E}_6 \\ \boldsymbol{E}_6 \\ \boldsymbol{E}_6 \end{bmatrix}, \quad \boldsymbol{V} = \frac{1}{3} \begin{bmatrix} -4\boldsymbol{E}_6 & -2\boldsymbol{E}_6 \\ 2\boldsymbol{E}_6 & -2\boldsymbol{E}_6 \\ 2\boldsymbol{E}_6 & 4\boldsymbol{E}_6 \end{bmatrix}.$$

Cooperation Between Two Humanoid Robots

Suppose two humanoid robots grasp an object with their hands. As illustrated in Fig. 6.14, the robot arms are numbered from 1 to 4. Since there are four robot arms ($p = 4$), the number of two-combinations is ${}_4C_2 = 4(4-1)/2 = 6$. Hence, there are six internal wrenches. They are denoted as $\mathcal{F}_{O_{12}}^I$, $\mathcal{F}_{O_{23}}^I$, $\mathcal{F}_{O_{34}}^I$, $\mathcal{F}_{O_{41}}^I$, $\mathcal{F}_{O_{13}}^I$, and $\mathcal{F}_{O_{24}}^I$. Note, however, that there will be only three independent internal wrenches (since $p - 1 = 4 - 1$).

Generally, the internal forces of importance in this case will be: (1) internal force $\mathcal{F}^I_{O_{AB}}$ between the two robots, (2) internal force $\mathcal{F}^I_{O_{12}}$ between arms 1 and 2, and (3) internal force $\mathcal{F}^I_{O_{34}}$ between Arms 3 and 4 (see Fig. 6.14).

Robot A applies two wrenches, $\mathcal{F}_{O_1}$ and $\mathcal{F}_{O_2}$, to point O_O by using Arms 1 and 2. The resultant wrench is $\mathcal{F}_{O_A} = \mathcal{F}_{O_1} + \mathcal{F}_{O_2}$. In the same way, Robot B applies the resultant force, $\mathcal{F}_{O_B} = \mathcal{F}_{O_3} + \mathcal{F}_{O_4}$, to point O_O by its Arms 3 and 4. Then, the internal force generated between the two robots can be defined as

$$\begin{aligned}\mathcal{F}^I_{O_{AB}} &= \frac{1}{2}\left(\mathcal{F}_{O_B} - \mathcal{F}_{O_A}\right) = \frac{1}{2}\left(\left(\mathcal{F}_{O_3} + \mathcal{F}_{O_4}\right) - \left(\mathcal{F}_{O_1} + \mathcal{F}_{O_2}\right)\right) \\ &= \mathcal{F}^I_{O_{13}} + \mathcal{F}^I_{O_{24}}.\end{aligned} \tag{6.71}$$

Note that the expression in the last row is the sum of internal forces defined in (6.67).

Internal wrench $\mathcal{F}^I_O$ can be defined as follows:

$$\mathcal{F}^I_O = \begin{bmatrix} \mathcal{F}^I_{O_{12}} \\ \mathcal{F}^I_{O_{34}} \\ \mathcal{F}^I_{O_{AB}} \end{bmatrix} = \boldsymbol{Q} \begin{bmatrix} \mathcal{F}_{O_1} \\ \mathcal{F}_{O_2} \\ \mathcal{F}_{O_3} \\ \mathcal{F}_{O_4} \end{bmatrix}, \tag{6.72}$$

$$\boldsymbol{Q} = \frac{1}{2}\begin{bmatrix} -\boldsymbol{E}_6 & \boldsymbol{E}_6 & \boldsymbol{0}_6 & \boldsymbol{0}_6 \\ \boldsymbol{0}_6 & \boldsymbol{0}_6 & -\boldsymbol{E}_6 & \boldsymbol{E}_6 \\ -\boldsymbol{E}_6 & -\boldsymbol{E}_6 & \boldsymbol{E}_6 & \boldsymbol{E}_6 \end{bmatrix}.$$

Substituting (6.40) and (6.72) into (6.65), the following equation is obtained:

$$\begin{bmatrix} \mathcal{F}^A_O \\ \mathcal{F}^I_{O_{12}} \\ \mathcal{F}^I_{O_{34}} \\ \mathcal{F}^I_{O_{AB}} \end{bmatrix} = \begin{bmatrix} \boldsymbol{E}_{6\times 6p} \\ \boldsymbol{Q} \end{bmatrix} \begin{bmatrix} \mathcal{F}_{O_1} \\ \mathcal{F}_{O_2} \\ \mathcal{F}_{O_3} \\ \mathcal{F}_{O_4} \end{bmatrix} = \begin{bmatrix} \boldsymbol{E}_6 & \boldsymbol{E}_6 & \boldsymbol{E}_6 & \boldsymbol{E}_6 \\ -\frac{1}{2}\boldsymbol{E}_6 & \frac{1}{2}\boldsymbol{E}_6 & \boldsymbol{0}_6 & \boldsymbol{0}_6 \\ \boldsymbol{0}_6 & \boldsymbol{0}_6 & -\frac{1}{2}\boldsymbol{E}_6 & \frac{1}{2}\boldsymbol{E}_6 \\ -\frac{1}{2}\boldsymbol{E}_6 & -\frac{1}{2}\boldsymbol{E}_6 & \frac{1}{2}\boldsymbol{E}_6 & \frac{1}{2}\boldsymbol{E}_6 \end{bmatrix} \begin{bmatrix} \mathcal{F}_{O_1} \\ \mathcal{F}_{O_2} \\ \mathcal{F}_{O_3} \\ \mathcal{F}_{O_4} \end{bmatrix}. \tag{6.73}$$

Given the desired wrench $(\mathcal{F}^A)^{des}$ to be impressed on the object and the desired internal forces $\mathcal{F}^I_{O_{12}}$, $\mathcal{F}^I_{O_{34}}$, and $\mathcal{F}^I_{O_{AB}}$, the desired hand wrenches $\mathcal{F}_{O_j}$ to be applied at point O_o are calculated as follows:

$$\begin{bmatrix} \mathcal{F}_{O_1} \\ \mathcal{F}_{O_2} \\ \mathcal{F}_{O_3} \\ \mathcal{F}_{O_4} \end{bmatrix} = \begin{bmatrix} \frac{1}{4}\boldsymbol{E}_6 & -\boldsymbol{E}_6 & \boldsymbol{0}_6 & -\frac{1}{2}\boldsymbol{E}_6 \\ \frac{1}{4}\boldsymbol{E}_6 & \boldsymbol{E}_6 & \boldsymbol{0}_6 & -\frac{1}{2}\boldsymbol{E}_6 \\ \frac{1}{4}\boldsymbol{E}_6 & \boldsymbol{0}_6 & -\boldsymbol{E}_6 & \frac{1}{2}\boldsymbol{E}_6 \\ \frac{1}{4}\boldsymbol{E}_6 & \boldsymbol{0}_6 & \boldsymbol{E}_6 & \frac{1}{2}\boldsymbol{E}_6 \end{bmatrix} \begin{bmatrix} \mathcal{F}^A_O \\ \mathcal{F}^I_{O_{12}} \\ \mathcal{F}^I_{O_{34}} \\ \mathcal{F}^I_{O_{AB}} \end{bmatrix} = \begin{bmatrix} \boldsymbol{E}^+_{6\times 6p} & \boldsymbol{V} \end{bmatrix} \begin{bmatrix} \mathcal{F}^A_O \\ \mathcal{F}^I_O \end{bmatrix}, \tag{6.74}$$

$$\mathcal{F}^I_O = \begin{bmatrix} \mathcal{F}^I_{O_{12}} \\ \mathcal{F}^I_{O_{34}} \\ \mathcal{F}^I_{O_{AB}} \end{bmatrix}, \quad \boldsymbol{E}^+_{6\times 6p} = \frac{1}{4}\begin{bmatrix} \boldsymbol{E}_6 \\ \boldsymbol{E}_6 \\ \boldsymbol{E}_6 \\ \boldsymbol{E}_6 \end{bmatrix}, \quad \boldsymbol{V} = \begin{bmatrix} -\boldsymbol{E}_6 & \boldsymbol{0}_6 & -\frac{1}{2}\boldsymbol{E}_6 \\ \boldsymbol{E}_6 & \boldsymbol{0}_6 & -\frac{1}{2}\boldsymbol{E}_6 \\ \boldsymbol{0}_6 & -\boldsymbol{E}_6 & \frac{1}{2}\boldsymbol{E}_6 \\ \boldsymbol{0}_6 & \boldsymbol{E}_6 & \frac{1}{2}\boldsymbol{E}_6 \end{bmatrix}.$$

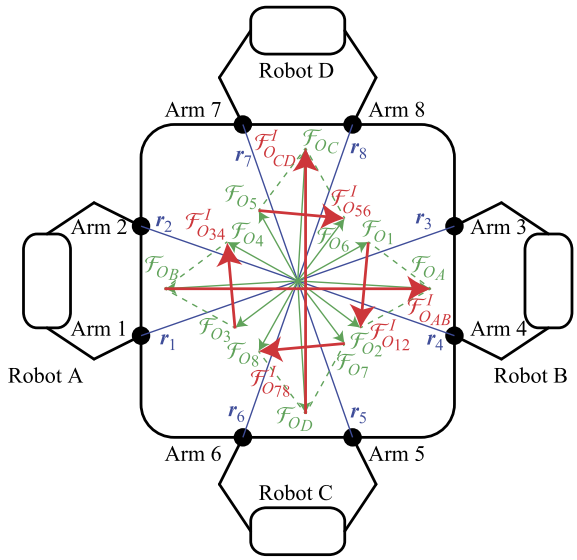

FIGURE 6.15 Cooperation among four humanoid robots.

The above wrenches are just particular solutions of the underdetermined wrench distribution problem. Other solutions can also be considered by choosing appropriate sums of internal forces (6.67).

Cooperation Among Four Humanoid Robots

The last example to be discussed is about cooperation among four humanoid robots. As illustrated in Fig. 6.15, the robot arms are numbered from 1 to 8. Since there are eight robot arms ($p = 8$), the number of two-combinations is ${}_8C_2 = 8(8-1)/2 = 28$. Thus, there will be 28 internal wrenches. Among them only seven ($p - 1 = 8 - 1$) will be independent, however. The remaining 21 wrenches will be dependent.

Generally, the important internal wrenches in this case will be: (1) internal force between two pairs of robots, e.g. between robots A and B and robots C and D, $\mathcal{F}^I_{O_{(AB)(CD)}}$; (2) the internal forces between the pair of robots facing each other, i.e. $\mathcal{F}^I_{O_{AB}}$ and $\mathcal{F}^I_{O_{CD}}$; and (3) internal forces $\mathcal{F}^I_{O_{12}}$, $\mathcal{F}^I_{O_{34}}$, $\mathcal{F}^I_{O_{56}}$, and $\mathcal{F}^I_{O_{78}}$ between the arms of each robot (see Fig. 6.15).

Robot A applies two wrenches $\mathcal{F}_{O_1}$ and $\mathcal{F}_{O_2}$ at point O_O by using Arms 1 and 2. The resultant wrench is given as $\mathcal{F}_{O_A} = \mathcal{F}_{O_1} + \mathcal{F}_{O_2}$. In the same way, Robots B, C, and D apply resultant wrenches $\mathcal{F}_{O_B} = \mathcal{F}_{O_3} + \mathcal{F}_{O_4}$, $\mathcal{F}_{O_C} = \mathcal{F}_{O_5} + \mathcal{F}_{O_6}$, and $\mathcal{F}_{O_D} = \mathcal{F}_{O_7} + \mathcal{F}_{O_8}$, respectively.

The internal force between the two pairs of robots, A–B and C–D, can be defined as follows:

$$\begin{aligned} \mathcal{F}^I_{O_{(AB)(CD)}} &= \frac{1}{2}\left(\mathcal{F}_{O_C} + \mathcal{F}_{O_D}\right) - \frac{1}{2}\left(\mathcal{F}_{O_A} + \mathcal{F}_{O_B}\right) \\ &= \frac{1}{2}\left(-\mathcal{F}_{O_1} - \mathcal{F}_{O_2} - \mathcal{F}_{O_3} - \mathcal{F}_{O_4} + \mathcal{F}_{O_5} + \mathcal{F}_{O_6} + \mathcal{F}_{O_7} + \mathcal{F}_{O_8}\right). \end{aligned} \tag{6.75}$$

The internal forces generated between the two pairs of robots, facing each other, can be expressed as

$$\mathcal{F}^I_{O_{AB}} = \frac{1}{2}\left(\mathcal{F}_{O_B} - \mathcal{F}_{O_A}\right) = \frac{1}{2}\left(-\mathcal{F}_{O_1} - \mathcal{F}_{O_2} + \mathcal{F}_{O_3} + \mathcal{F}_{O_4}\right), \tag{6.76}$$

$$\mathcal{F}^I_{O_{CD}} = \frac{1}{2}\left(\mathcal{F}_{O_D} - \mathcal{F}_{O_C}\right) = \frac{1}{2}\left(-\mathcal{F}_{O_5} - \mathcal{F}_{O_6} + \mathcal{F}_{O_7} + \mathcal{F}_{O_8}\right). \tag{6.77}$$

Furthermore, $\mathcal{F}^I_{O_{(AB)(CD)}}$, $\mathcal{F}^I_{O_{AB}}$, and $\mathcal{F}^I_{O_{CD}}$ can be represented as sums of internal forces (cf. (6.67)), i.e.

$$\begin{aligned}
\mathcal{F}^I_{O_{(AB)(CD)}} &= \mathcal{F}^I_{O_{15}} + \mathcal{F}^I_{O_{26}} + \mathcal{F}^I_{O_{37}} + \mathcal{F}^I_{O_{48}},\\
\mathcal{F}^I_{O_{AB}} &= \mathcal{F}^I_{O_{13}} + \mathcal{F}^I_{O_{24}},\\
\mathcal{F}^I_{O_{CD}} &= \mathcal{F}^I_{O_{57}} + \mathcal{F}^I_{O_{68}},
\end{aligned}$$

respectively.

Internal forces $\mathcal{F}^I_O$ can be defined as follows:

$$\mathcal{F}^I_O = \boldsymbol{Q}\mathcal{F}_O, \tag{6.78}$$

$$\mathcal{F}^I_O = \begin{bmatrix} \mathcal{F}^I_{O_{(AB)(CD)}} & \mathcal{F}^I_{O_{AB}} & \mathcal{F}^I_{O_{CD}} & \mathcal{F}^I_{O_{12}} & \mathcal{F}^I_{O_{34}} & \mathcal{F}^I_{O_{56}} & \mathcal{F}^I_{O_{78}} \end{bmatrix}^T,$$

$$\mathcal{F}_O = \begin{bmatrix} \mathcal{F}_{O_1} & \mathcal{F}_{O_2} & \mathcal{F}_{O_3} & \mathcal{F}_{O_4} & \mathcal{F}_{O_5} & \mathcal{F}_{O_6} & \mathcal{F}_{O_7} & \mathcal{F}_{O_8} \end{bmatrix}^T,$$

$$\boldsymbol{Q} = \frac{1}{2}\begin{bmatrix}
-\boldsymbol{E}_6 & -\boldsymbol{E}_6 & -\boldsymbol{E}_6 & -\boldsymbol{E}_6 & \boldsymbol{E}_6 & \boldsymbol{E}_6 & \boldsymbol{E}_6 & \boldsymbol{E}_6\\
-\boldsymbol{E}_6 & -\boldsymbol{E}_6 & \boldsymbol{E}_6 & \boldsymbol{E}_6 & \boldsymbol{0}_6 & \boldsymbol{0}_6 & \boldsymbol{0}_6 & \boldsymbol{0}_6\\
\boldsymbol{0}_6 & \boldsymbol{0}_6 & \boldsymbol{0}_6 & \boldsymbol{0}_6 & -\boldsymbol{E}_6 & -\boldsymbol{E}_6 & \boldsymbol{E}_6 & \boldsymbol{E}_6\\
-\boldsymbol{E}_6 & \boldsymbol{E}_6 & \boldsymbol{0}_6 & \boldsymbol{0}_6 & \boldsymbol{0}_6 & \boldsymbol{0}_6 & \boldsymbol{0}_6 & \boldsymbol{0}_6\\
\boldsymbol{0}_6 & \boldsymbol{0}_6 & -\boldsymbol{E}_6 & \boldsymbol{E}_6 & \boldsymbol{0}_6 & \boldsymbol{0}_6 & \boldsymbol{0}_6 & \boldsymbol{0}_6\\
\boldsymbol{0}_6 & \boldsymbol{0}_6 & \boldsymbol{0}_6 & \boldsymbol{0}_6 & -\boldsymbol{E}_6 & \boldsymbol{E}_6 & \boldsymbol{0}_6 & \boldsymbol{0}_6\\
\boldsymbol{0}_6 & \boldsymbol{0}_6 & \boldsymbol{0}_6 & \boldsymbol{0}_6 & \boldsymbol{0}_6 & \boldsymbol{0}_6 & -\boldsymbol{E}_6 & \boldsymbol{E}_6
\end{bmatrix}.$$

Substituting (6.40) and (6.78) into (6.65), the following equation is obtained:

$$\begin{aligned}
\begin{bmatrix} \mathcal{F}^A_O \\ \mathcal{F}^I_O \end{bmatrix} &= \begin{bmatrix} \boldsymbol{E}_{6\times 6p} \\ \boldsymbol{Q} \end{bmatrix}\mathcal{F}_O\\
&= \begin{bmatrix}
\boldsymbol{E}_6 & \boldsymbol{E}_6 & \boldsymbol{E}_6 & \boldsymbol{E}_6 & \boldsymbol{E}_6 & \boldsymbol{E}_6 & \boldsymbol{E}_6 & \boldsymbol{E}_6\\
-\frac{1}{2}\boldsymbol{E}_6 & -\frac{1}{2}\boldsymbol{E}_6 & -\frac{1}{2}\boldsymbol{E}_6 & -\frac{1}{2}\boldsymbol{E}_6 & \frac{1}{2}\boldsymbol{E}_6 & \frac{1}{2}\boldsymbol{E}_6 & \frac{1}{2}\boldsymbol{E}_6 & \frac{1}{2}\boldsymbol{E}_6\\
-\frac{1}{2}\boldsymbol{E}_6 & -\frac{1}{2}\boldsymbol{E}_6 & \frac{1}{2}\boldsymbol{E}_6 & \frac{1}{2}\boldsymbol{E}_6 & \boldsymbol{0}_6 & \boldsymbol{0}_6 & \boldsymbol{0}_6 & \boldsymbol{0}_6\\
\boldsymbol{0}_6 & \boldsymbol{0}_6 & \boldsymbol{0}_6 & \boldsymbol{0}_6 & -\frac{1}{2}\boldsymbol{E}_6 & -\frac{1}{2}\boldsymbol{E}_6 & \frac{1}{2}\boldsymbol{E}_6 & \frac{1}{2}\boldsymbol{E}_6\\
-\frac{1}{2}\boldsymbol{E}_6 & \frac{1}{2}\boldsymbol{E}_6 & \boldsymbol{0}_6 & \boldsymbol{0}_6 & \boldsymbol{0}_6 & \boldsymbol{0}_6 & \boldsymbol{0}_6 & \boldsymbol{0}_6\\
\boldsymbol{0}_6 & \boldsymbol{0}_6 & -\frac{1}{2}\boldsymbol{E}_6 & \frac{1}{2}\boldsymbol{E}_6 & \boldsymbol{0}_6 & \boldsymbol{0}_6 & \boldsymbol{0}_6 & \boldsymbol{0}_6\\
\boldsymbol{0}_6 & \boldsymbol{0}_6 & \boldsymbol{0}_6 & \boldsymbol{0}_6 & -\frac{1}{2}\boldsymbol{E}_6 & \frac{1}{2}\boldsymbol{E}_6 & \boldsymbol{0}_6 & \boldsymbol{0}_6\\
\boldsymbol{0}_6 & \boldsymbol{0}_6 & \boldsymbol{0}_6 & \boldsymbol{0}_6 & \boldsymbol{0}_6 & \boldsymbol{0}_6 & -\frac{1}{2}\boldsymbol{E}_6 & \frac{1}{2}\boldsymbol{E}_6
\end{bmatrix}\begin{bmatrix} \mathcal{F}_{O_1} \\ \mathcal{F}_{O_2} \\ \mathcal{F}_{O_3} \\ \mathcal{F}_{O_4} \\ \mathcal{F}_{O_5} \\ \mathcal{F}_{O_6} \\ \mathcal{F}_{O_7} \\ \mathcal{F}_{O_8} \end{bmatrix}.
\end{aligned} \tag{6.79}$$

Given the desired wrench to be applied, $(\mathcal{F}_O^A)^{des}$, and the desired internal forces, $\mathcal{F}_O^{I,\,des}$, the desired wrench to be applied by Arm j at point O_O is calculated as

$$\begin{bmatrix} \mathcal{F}_{O_1} \\ \mathcal{F}_{O_2} \\ \mathcal{F}_{O_3} \\ \mathcal{F}_{O_4} \\ \mathcal{F}_{O_5} \\ \mathcal{F}_{O_6} \\ \mathcal{F}_{O_7} \\ \mathcal{F}_{O_8} \end{bmatrix} = \begin{bmatrix} \frac{1}{8}\boldsymbol{E}_6 & -\frac{1}{4}\boldsymbol{E}_6 & -\frac{1}{2}\boldsymbol{E}_6 & \boldsymbol{0}_6 & -\boldsymbol{E}_6 & \boldsymbol{0}_6 & \boldsymbol{0}_6 & \boldsymbol{0}_6 \\ \frac{1}{8}\boldsymbol{E}_6 & -\frac{1}{4}\boldsymbol{E}_6 & -\frac{1}{2}\boldsymbol{E}_6 & \boldsymbol{0}_6 & \boldsymbol{E}_6 & \boldsymbol{0}_6 & \boldsymbol{0}_6 & \boldsymbol{0}_6 \\ \frac{1}{8}\boldsymbol{E}_6 & -\frac{1}{4}\boldsymbol{E}_6 & \frac{1}{2}\boldsymbol{E}_6 & \boldsymbol{0}_6 & \boldsymbol{0}_6 & -\boldsymbol{E}_6 & \boldsymbol{0}_6 & \boldsymbol{0}_6 \\ \frac{1}{8}\boldsymbol{E}_6 & -\frac{1}{4}\boldsymbol{E}_6 & \frac{1}{2}\boldsymbol{E}_6 & \boldsymbol{0}_6 & \boldsymbol{0}_6 & \boldsymbol{E}_6 & \boldsymbol{0}_6 & \boldsymbol{0}_6 \\ \frac{1}{8}\boldsymbol{E}_6 & \frac{1}{4}\boldsymbol{E}_6 & \boldsymbol{0}_6 & -\frac{1}{2}\boldsymbol{E}_6 & \boldsymbol{0}_6 & \boldsymbol{0}_6 & -\boldsymbol{E}_6 & \boldsymbol{0}_6 \\ \frac{1}{8}\boldsymbol{E}_6 & \frac{1}{4}\boldsymbol{E}_6 & \boldsymbol{0}_6 & -\frac{1}{2}\boldsymbol{E}_6 & \boldsymbol{0}_6 & \boldsymbol{0}_6 & \boldsymbol{E}_6 & \boldsymbol{0}_6 \\ \frac{1}{8}\boldsymbol{E}_6 & \frac{1}{4}\boldsymbol{E}_6 & \boldsymbol{0}_6 & \frac{1}{2}\boldsymbol{E}_6 & \boldsymbol{0}_6 & \boldsymbol{0}_6 & \boldsymbol{0}_6 & -\boldsymbol{E}_6 \\ \frac{1}{8}\boldsymbol{E}_6 & \frac{1}{4}\boldsymbol{E}_6 & \boldsymbol{0}_6 & \frac{1}{2}\boldsymbol{E}_6 & \boldsymbol{0}_6 & \boldsymbol{0}_6 & \boldsymbol{0}_6 & \boldsymbol{E}_6 \end{bmatrix} \begin{bmatrix} \mathcal{F}_O^A \\ \mathcal{F}_{O_{(AB)(CD)}}^I \\ \mathcal{F}_{O_{AB}}^I \\ \mathcal{F}_{O_{CD}}^I \\ \mathcal{F}_{O_{12}}^I \\ \mathcal{F}_{O_{34}}^I \\ \mathcal{F}_{O_{56}}^I \\ \mathcal{F}_{O_{78}}^I \end{bmatrix}. \tag{6.80}$$

The above wrenches are just particular solutions of the underdetermined wrench distribution problem. Other solutions can also be considered by choosing appropriate sums of internal forces.

6.3.6 Hybrid Position/Force Control

Cooperation among multiple robot arms based on force control was discussed in Section 6.3.5. This section discusses a position/force hybrid control approach for the case of multirobot cooperation. The deformation of the object and possible slippage between the object and the hands are not considered here. As discussed in Section 6.3.2, the position and orientation, $\boldsymbol{r}_{O_j}$ and $\boldsymbol{R}_{O_j}$ (see Fig. 6.7), generally correspond to those of the object at O_O, i.e. $\boldsymbol{r}_O$ and $\boldsymbol{R}_O$.

Suppose that p robot arms grasp an object, applying thereby the net wrench $\mathcal{F}_O$. The relationship between $\mathcal{F}_O$ and the resultant wrenches, i.e. external wrench $\mathcal{F}_O^A$ and internal wrench $\mathcal{F}_O^I$, is calculated from (6.42). Making use of the principle of virtual work, the following equation can be obtained:

$$\begin{bmatrix} \left(\mathcal{F}_O^A\right)^T & \left(\mathcal{F}_O^I\right)^T \end{bmatrix} \begin{bmatrix} \delta\mathcal{X}_O^A \\ \delta\mathcal{X}_O^I \end{bmatrix} = \mathcal{F}_O^T \delta\mathcal{X}_O, \tag{6.81}$$

$$\delta\mathcal{X}_O^I \equiv \begin{bmatrix} \delta\mathcal{X}_{O_1}^I \\ \vdots \\ \delta\mathcal{X}_{O_{(p-1)}}^I \end{bmatrix} \in \Re^{6(p-1)}, \quad \delta\mathcal{X}_O \equiv \begin{bmatrix} \delta\mathcal{X}_{O_1} \\ \vdots \\ \delta\mathcal{X}_{O_p} \end{bmatrix} \in \Re^{6p}.$$

Here $\delta\mathcal{X}_O^A$ is the small displacement of the object, $\delta\mathcal{X}_O^I$ is the stacked relative displacements caused by internal force $\mathcal{F}_O^I$, and $\delta\mathcal{X}_O$ are stacked displacement vectors $\delta\mathcal{X}_{O_j}$ defined in (6.37).

From (6.42) and (6.81), the small 6D displacement caused by external wrench $\mathcal{F}_O^A$ and internal wrench $\mathcal{F}_O^I$ is given as

$$\begin{aligned} \delta\mathcal{X}_O^{AI} &= \boldsymbol{U}^T \delta\mathcal{X}_O, \\ \delta\mathcal{X}_O^{AI} &\equiv \begin{bmatrix} \delta\mathcal{X}_O^A \\ \delta\mathcal{X}_O^I \end{bmatrix}, \end{aligned} \tag{6.82}$$

matrix $\boldsymbol{U}$ being defined in (6.66).

Position Controller

Given the desired position $\boldsymbol{r}_O^{des}$ and orientation $\boldsymbol{R}_O^{des}$ of the object, the position error is calculated from

$$\left(\delta\mathcal{X}_O^A\right)_{\mathcal{X}} = \begin{bmatrix} \boldsymbol{r}_O^{des} - \boldsymbol{r}_O \\ \left(\ln\ \boldsymbol{R}_O^T \boldsymbol{R}_O^{des}\right)^\vee \end{bmatrix}. \tag{6.83}$$

The internal wrench can also be controlled, by determining appropriate desired relative positions among the robot arms. If the desired relative position along the lth internal wrench, $\mathcal{F}_{O_l}^I$ $(1 \le l \le p-1)$, is given, the error in the relative position is calculated as follows:

$$\left(\delta\mathcal{X}_{O_l}^I\right)_{\mathcal{X}} = \begin{bmatrix} \boldsymbol{r}_{O_l}^{des} - \boldsymbol{r}_{O_l} \\ \left(\ln\ \boldsymbol{R}_{O_l}^T \boldsymbol{R}_{O_l}^{des}\right)^\vee \end{bmatrix}. \tag{6.84}$$

The superscript *des* denotes a desired state.

Given $\left(\delta\mathcal{X}_{O_l}^I\right)_{\mathcal{X}} = \mathbf{0}_6$, the corresponding robot arms are controlled to maintain the kinematic constraints; hence $\mathcal{F}_{O_l}^I$ is controlled to be zero.

Position-Based Force Controller

The reference position for force control is given by

$$\left(\delta\mathcal{X}_O^{AI}\right)_{\mathcal{F}} = \boldsymbol{K}_{\mathcal{F}}^{AI} \left\{ \left(\mathcal{F}_O^{AI}\right)^{des} - \left(\mathcal{F}_O^{AI}\right) \right\}, \tag{6.85}$$

where $\boldsymbol{K}_{\mathcal{F}}^{AI}$ is a diagonal gain matrix and $\mathcal{F}_O^{AI}$ is transformed from $\mathcal{F}_O$ using (6.65).

Hybrid Position/Force Controller

In most cases of multirobot cooperation it is desirable to control the position of the object and the internal wrenches distributed among the robots. The following position/force hybrid force controller can be employed in this case:

$$\left(\delta\mathcal{X}_O^{AI}\right)_{hybrid} = (\boldsymbol{E}_{6n} - \boldsymbol{S}) \left(\delta\mathcal{X}_O^{AI}\right)_{\mathcal{X}} + \boldsymbol{S} \left(\delta\mathcal{X}_O^{AI}\right)_{\mathcal{F}}, \tag{6.86}$$

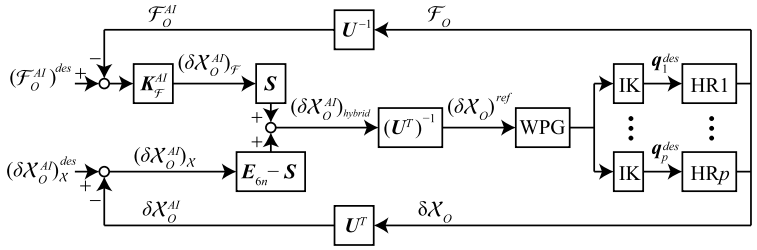

FIGURE 6.16 Position/force hybrid controller for multirobot cooperation. WPG, IK, and HRj denote walking pattern generator, inverse kinematics, and jth humanoid robot, respectively.

where $\boldsymbol{S}$ is a selection matrix. The reference position obtained from the above controller can be used to determine the reference tip positions of the virtual sticks, i.e.

$$\begin{bmatrix} \delta\mathcal{X}_{O_1}^{ref} \\ \vdots \\ \delta\mathcal{X}_{O_p}^{ref} \end{bmatrix} = \left(\boldsymbol{U}^T\right)^{-1} \left(\delta\mathcal{X}_O^{AI}\right)_{hybrid}. \tag{6.87}$$

The desired joint angles of the jth robot arm can then be obtained via the instantaneous kinematics relations (cf. (6.37)) as follows:

$$\boldsymbol{q}_j^{des} = \boldsymbol{J}_{O_j}^{+} \delta\mathcal{X}_{O_j}^{ref} + \boldsymbol{q}_j. \tag{6.88}$$

The block diagram of the position/force controller is illustrated in Fig. 6.16.

6.4 COOPERATION BETWEEN MULTIPLE HUMANOIDS

6.4.1 On-Line Footstep Planning

This section introduces a footstep planning method for cooperative object manipulation, as proposed in [30]. The concept is shown in Fig. 6.17. The planning of the footsteps is done for each robot separately. After grasping the object, each robot calculates the distances between the ground projection of the mid-point between the hands and the origins of the foot positions ($\boldsymbol{d}_1$ and $\boldsymbol{d}_2$, as illustrated in Fig. 6.17). When the robots start to move the object, the reference foot positions $\boldsymbol{d}_1^{des}$ and $\boldsymbol{d}_2^{des}$ are continuously calculated. When the error between the reference and the current foot position exceeds a specified threshold, the robot starts to walk. Once the reference foot position is decided, the reference zero-moment point (ZMP) trajectory is obtained by interpolating the discrete foot positions between the current and the reference ones. The reference CoM trajectory is computed using the preview control theory [9]. The robots stop walking when their foot position errors become lower than the threshold. The error includes the position error, e_{p}, and the attitude error in the yaw direction, e_{A}. These

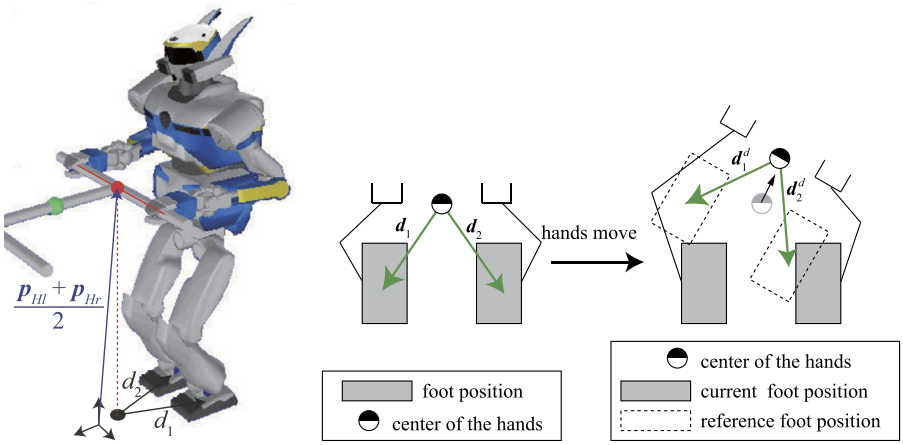

FIGURE 6.17 Concept of on-line footstep planning.

errors are defined as

$$e_{pk} = ||\boldsymbol{d}_k^{des} - \boldsymbol{d}_k||,$$
$$e_{Ak} = |\psi_k^{des} - \psi_k|,$$

where $k = 1, 2$ denotes the foot number and $\boldsymbol{d}_k^{des}$ and ψ_k^{des} are the desired position and yaw angle, respectively, and e_{pk} and e_{Ak} are checked after every step to make a decision about initializing another step or terminating the stepping.

The relative position error between the robots can be successfully compensated since the internal force of the system is controlled by stretching or shrinking the arms and since the desired foot position of the robot is calculated from the mid-point between the hands.

6.4.2 Coordinated Movement of Hands and Feet

Suppose the reference position $\left(\delta\mathcal{X}_O^{AI}\right)_{hybrid}^{ref}$ is given by the hybrid controller (6.86). The corresponding 6D positions of the virtual sticks for the two hands of the humanoid robot, $\delta\mathcal{X}_{O_j}^{ref}$ and $\delta\mathcal{X}_{O_{j+1}}^{ref}$, are calculated from (6.87).

As illustrated in Fig. 6.18, a humanoid robot walks swaying its CoM. However, the hand position must be controlled independently of the swaying motion.

The positions of the hands, ${}^{F_{st}}\delta\mathcal{X}_{H_l}^{ref}$ and ${}^{F_{st}}\delta\mathcal{X}_{H_r}^{ref}$, are defined w.r.t. the stance foot coordinate frame $\{F_{st}\}$. These positions are calculated from the positions of the virtual sticks $\delta\mathcal{X}_{O_j}^{ref}$ and $\delta\mathcal{X}_{O_{j+1}}^{ref}$.

Then, $\boldsymbol{d}_1$ and $\boldsymbol{d}_2$ can be calculated by using ${}^{F_{st}}\delta\mathcal{X}_{H_l}^{ref}$ and ${}^{F_{st}}\delta\mathcal{X}_{H_r}^{ref}$, as discussed in Section 6.4.1. In the case when e_{pk} or e_{Ak} exceeds the previously specified threshold, the on-line walking pattern generator defines the desired CoM and the trajectory of the swing foot.

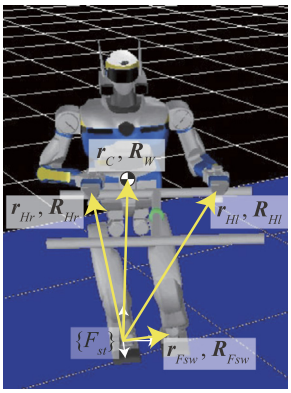

FIGURE 6.18 Position control of the hands, swing foot, and CoM.

Hence, the constraints can be summarized as: (1) the positions of the hands, (2) the CoM, and (3) the position of the swing foot.

The instantaneous kinematics equation (6.88) is therefore rewritten using the stacked Jacobian matrix and the stacked error vectors as follows:

$$\boldsymbol{q}_j^{des} = {}^{F_{st}}\underline{\boldsymbol{J}}_j^{+}\, {}^{F_{st}}\underline{\delta\mathcal{X}}_j^{ref} + \boldsymbol{q}_j, \tag{6.89}$$

where

$${}^{F_{st}}\underline{\boldsymbol{J}}_j = \begin{bmatrix} {}^{F_{st}}\boldsymbol{J}_C \\ {}^{F_{st}}\boldsymbol{J}_{F_{sw}} \\ {}^{F_{st}}\boldsymbol{J}_{H_l} \\ {}^{F_{st}}\boldsymbol{J}_{H_r} \end{bmatrix},$$

$${}^{F_{st}}\underline{\delta\mathcal{X}}_j^{ref} = \begin{bmatrix} {}^{F_{st}}\delta\mathcal{X}_C^{ref} \\ {}^{F_{st}}\delta\mathcal{X}_{F_{sw}}^{ref} \\ {}^{F_{st}}\delta\mathcal{X}_{H_l}^{ref} \\ {}^{F_{st}}\delta\mathcal{X}_{H_r}^{ref} \end{bmatrix},$$

$${}^{F_{st}}\delta\mathcal{X}_C^{ref} = \begin{bmatrix} {}^{F_{st}}\boldsymbol{r}_C^{des} - {}^{F_{st}}\boldsymbol{r}_C \\ \left(\ln {}^{F_{st}}\boldsymbol{R}_C^T\, {}^{F_{st}}\boldsymbol{R}_C^{des}\right)^{\vee} \end{bmatrix},$$

$${}^{F_{st}}\delta\mathcal{X}_{F_{sw}}^{ref} = \begin{bmatrix} {}^{F_{st}}\boldsymbol{r}_{F_{sw}}^{des} - {}^{F_{st}}\boldsymbol{r}_{F_{sw}} \\ \left(\ln {}^{F_{st}}\boldsymbol{R}_{F_{sw}}^T\, {}^{F_{st}}\boldsymbol{R}_{F_{sw}}^{des}\right)^{\vee} \end{bmatrix},$$

$${}^{F_{st}}\delta\mathcal{X}_{H_e}^{ref} = \begin{bmatrix} {}^{F_{st}}\boldsymbol{r}_{H_e}^{des} - {}^{F_{st}}\boldsymbol{r}_{H_e} \\ \left(\ln {}^{F_{st}}\boldsymbol{R}_{H_e}^T\, {}^{F_{st}}\boldsymbol{R}_{H_e}^{des}\right)^{\vee} \end{bmatrix}, \ (e = l \text{ or } r).$$

The control variables are listed below.

$\boldsymbol{r}_C$	position vector of the CoM
$\boldsymbol{R}_C$	rotation matrix of the CoM (actually of the waist)
$\boldsymbol{r}_{F_{sw}}$	position vector of the swing foot
$\boldsymbol{R}_{F_{sw}}$	rotation matrix of the swing foot
$\boldsymbol{r}_{F_{He}}$	position vector of the hand ($e = l$ or r)
$\boldsymbol{R}_{F_{He}}$	rotation matrix of the hand ($e = l$ or r)
$\boldsymbol{q}_j$	joint angular velocity vector of the whole body
$\boldsymbol{J}_C$	analytical Jacobian matrix that relates $\delta\boldsymbol{q}$ to $\delta\mathcal{X}_C$
$\boldsymbol{J}_{F_{sw}}$	analytical Jacobian matrix that relates $\delta\boldsymbol{q}$ to $\delta\mathcal{X}_{F_{sw}}$
$\boldsymbol{J}_{H_e}$	analytical Jacobian matrix that relates $\delta\boldsymbol{q}$ to $\delta\mathcal{X}_{F_{He}}$ ($e = l$ or r)

The trailing superscript des represents the desired state. The trailing superscript ref denotes the difference between the desired and the current states.

The meaning of the leading superscript F_{st} ($st = l$ or r) is that the vector or the matrix is defined w.r.t. the stance foot coordinate frame $\{F_{st}\}$ ($st = l$ or r). Since the left and right foot alternately play the role of the stance foot, two different sets of Jacobian matrices and reference vectors, i.e. $({}^{F_l}\underline{\boldsymbol{J}}_j,\ {}^{F_l}\underline{\delta\mathcal{X}}_j)$ and $({}^{F_r}\underline{\boldsymbol{J}}_j,\ {}^{F_r}\underline{\delta\mathcal{X}}_j)$, have to be used alternately. When the robot is in the double-support phase, the inverse kinematics are solved by letting ${}^{F_{st}}\delta\mathcal{X}^{ref}_{F_{sw}} = \boldsymbol{0}_6$.

6.4.3 Leader-Follower- and Symmetry-Type Cooperation

The multiarm object manipulation control method discussed in Section 6.3 can be applied to the problem of cooperating humanoid robots. Multirobot cooperation is classified into (a) leader-follower-type cooperation and (b) symmetry-type cooperation. The concepts of these two types of cooperation are visualized in Fig. 6.19.

In leader-follower-type cooperation, one of the robots behaves as a leader while the remaining robots behave as followers. The leader robot controls the position and orientation of the grasped object while the followers control the internal wrenches. Generally, only the gravitational force of the grasped object is distributed to all robots. The motion of the object along the other five axes is controlled by the leader robot.

In symmetry-type cooperation, on the other hand, all robots equally control the motion of the grasped object and the internal forces.

Implementations of leader-follower-type cooperation and symmetry-type cooperation are presented in the following subsections.

6.4.4 Leader-Follower-Type Cooperative Object Manipulation

This section introduces a method of a leader-follower-type cooperative object manipulation, as proposed in [30]. The method applies to humanoid robots comprising gear drives with high reduction ratios and hardware joint-position servos. Most of the actual humanoid

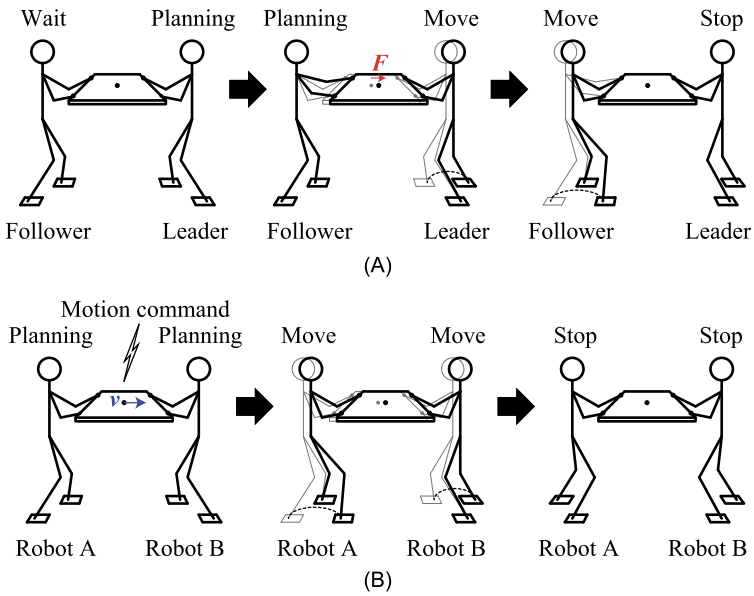

FIGURE 6.19 Two types of multirobot cooperation. (A) Concept of leader-follower-type cooperation. (B) Concept of symmetry-type cooperation.

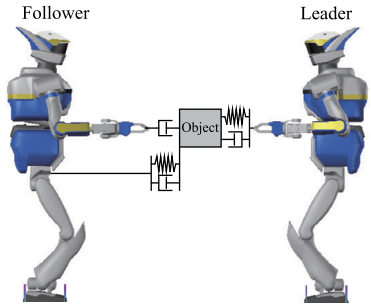

FIGURE 6.20 Concept of a leader-follower-type cooperation.

robots fall within this category. They accept control commands specified in terms of joint positions.

Concept of a Leader-Follower-Type Cooperative Object Manipulation

Generally, the leader robot controls the position (or motion) of the carried object and the follower robots control the internal force. The concept of leader-follower-type cooperation proposed in [30] is illustrated in Fig. 6.20. The leader robot walks in the direction commanded to carry the object. The motion of its arms is determined by an impedance control law. The motion of the arms of the follower robots, on the other hand, is determined by a damping con-

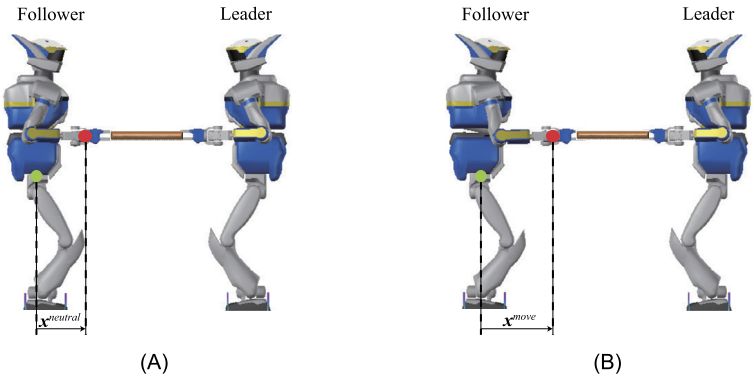

FIGURE 6.21 Time lag between the movements of the leader and the follower robots. (A) Neutral hand position. (B) Hand position after the leader moves.

trol law. The walking gaits of the robots are generated on-line, assuming virtual springs and dampers between the object and the robots, as illustrated in Fig. 6.20. Thereby, the distance between the grasped object and the follower robots is controlled by the generated walking gait.

When the leader robot moves the grasped object, the hands of the follower robot are stretched under the damping control. Let $\mathcal{X}^{neutral}$ and $\mathcal{X}^{move}$ be the neutral hand position of the follower robot and the hand position after the leader robot moves, respectively, as illustrated in Fig. 6.21. The difference between $\mathcal{X}^{neutral}$ and $\mathcal{X}^{move}$ is defined by $\Delta\mathcal{X} = \mathcal{X}^{move} - \mathcal{X}^{neutral}$. A PD controller is designed to generate a step that controls $\Delta\mathcal{X}$ to zero as follows:

$$\mathcal{X}^{step} = \boldsymbol{K}_{Pstep}\Delta\mathcal{X} + \boldsymbol{K}_{Dstep}\Delta\dot{\mathcal{X}}. \tag{6.90}$$

Here $\mathcal{X}^{step}$ is the next desired footprint with respect to the current stance foot; $\boldsymbol{K}_{Pstep}$ and $\boldsymbol{K}_{Dstep}$ act as a virtual spring and damper, respectively, as illustrated in Fig. 6.20. The reference ZMP is computed in accordance with the walking command. The CoM trajectory can then be calculated with the help of the preview control approach [9].

Experiment of Object Transportation

Results from the leader-follower-type cooperative object manipulation experiment reported in [30] are presented in this section. The goal was to carry the object in the direction of the x-axis (see Fig. 6.22A for the coordinate frame). The commanded object positions along the y- and z-axes were constant.

In the experiment, the leader robot first walked backward, thus moving the grasped object in its direction. Then, the direction of the movement was changed and the leader robot moved the object in the direction of the follower robot, while walking forward. Snapshots from the movements of the leader and follower robots are presented in Fig. 6.22. More detailed data, such as hand positions and forces generated during the experiment, are given in [30].

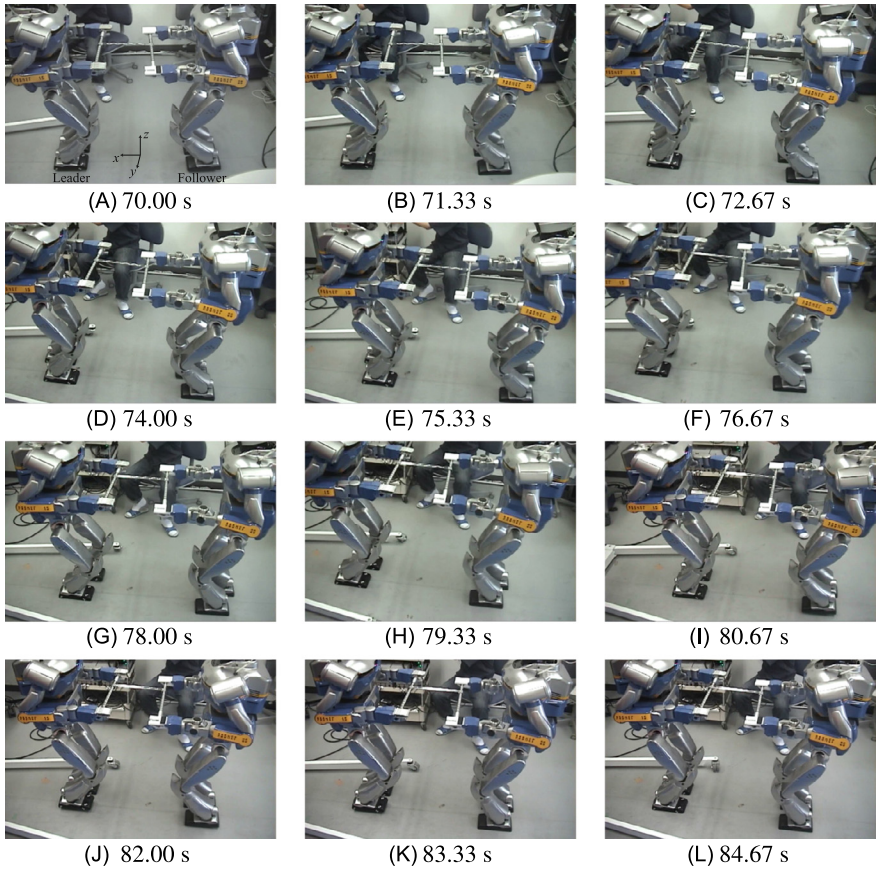

FIGURE 6.22 Cooperative object transportation by two humanoid robots [30].

6.4.5 Symmetry-Type Cooperative Object Manipulation

The multiarm object manipulation control method introduced in Section 6.3 is applied to control the cooperation between multiple humanoid robots. In what follows, cooperative object manipulation between two humanoid robots will be discussed.

Simulation of Symmetry-Type Cooperation

An example of symmetry-type cooperation between two humanoid robots is illustrated in Fig. 6.14. Given the desired applied wrench, $\mathcal{F}^{A,des}$, and the desired internal wrenches, $\mathcal{F}^I_{O_{12}}$, $\mathcal{F}^I_{O_{34}}$, and $\mathcal{F}^I_{O_{AB}}$, the desired hand wrenches $\mathcal{F}^{des}_{O_j}$ can be calculated from (6.74).

In the simulation experiment for symmetry-type cooperation, two models of the humanoid robot HRP-2 [11] were used. OpenHRP-3 [10] was used for the dynamic simulation.

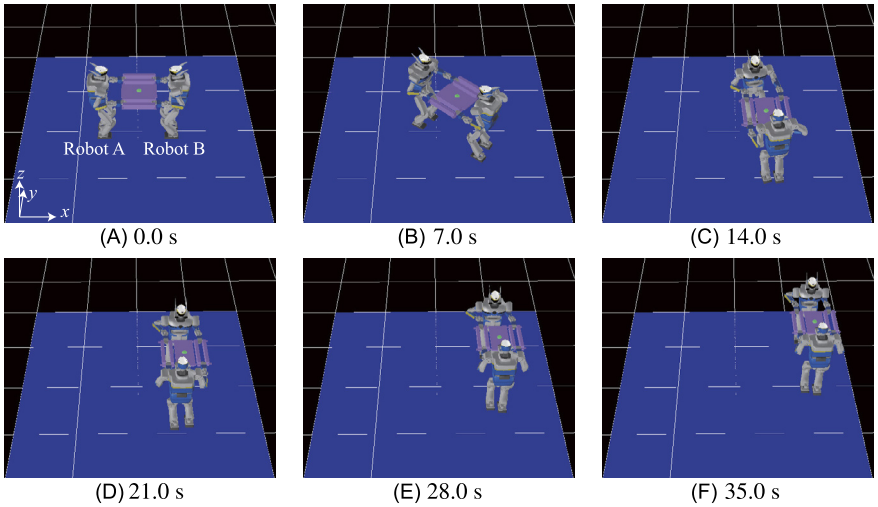

FIGURE 6.23 Snapshots from on-line operation [29].

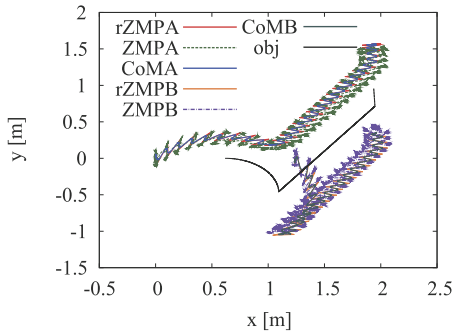

FIGURE 6.24 Result of on-line operation [29].

Video 6.4-1 [12] shows the simulation results from the cooperative motion of four humanoid robots.

Simulation Results

The snapshots in Fig. 6.23 are from the movement of two humanoid robots during the simulation of cooperative object transportation. Fig. 6.24 shows the trajectory of the reference ZMP (rZMP), ZMP, CoM, and the object. Fig. 6.25 shows the internal wrench $\mathcal{F}^I_{O_{AB}}$ generated during the simulation. This wrench is defined in (6.71). When the internal wrench is not controlled, spikes of the internal wrench are observed especially in the x-direction, as shown in Fig. 6.25. The spikes of the internal wrench are well reduced by applying force control.

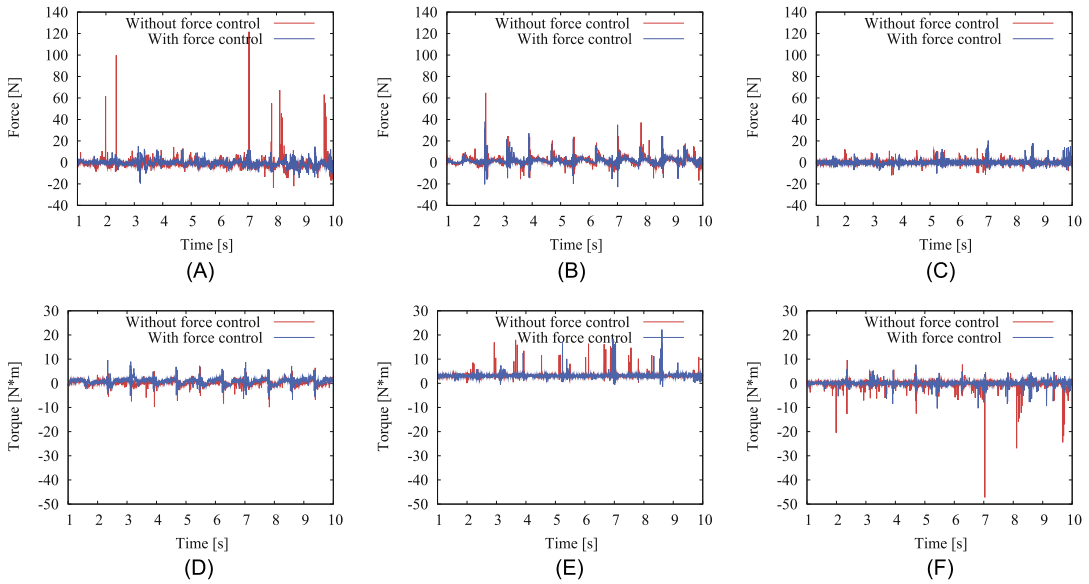

FIGURE 6.25 Internal wrench generated at the object [29]. (A) Internal force along the x-axis. (B) Internal force along the y-axis. (C) Internal force along the z-axis. (D) Internal moment around the x-axis. (E) Internal moment around the y-axis. (F) Internal moment around the z-axis.

6.4.6 Comparison Between Leader-Follower-Type and Symmetry-Type Cooperation

A comparison between the symmetry-type cooperation and the leader-follower-type cooperation based on a dynamic simulation is discussed in this section. In the simulation, the same constant reference velocity of 0.1 m/s is given for the object along the x-axis. Figs. 6.26 and 6.27 show the snapshots of the dynamic simulation of the leader-follower-type cooperation and the symmetry-type cooperation, respectively. The ZMP trajectories during the simulation are plotted in Fig. 6.28.

In the simulation of the leader-follower-type cooperation, the leader robot lost the balance because of the time lag between the leader and the follower robot, as shown in Fig. 6.26C. The leader robot moved first; then the follower robot moved, but the follower robot could not respond quickly enough. The ZMP in the x-axis went to the front fringe of the support polygon at $t = 7.2$ s, as shown in Fig. 6.28A.

In the symmetry-type cooperation, the two robots stably transported the object, as shown in Fig. 6.27. The ZMP always stayed near the center of the support polygon, as shown in Fig. 6.28B.

The results show that the symmetry-type cooperation is more stable for biped robots than the leader-follower-type cooperation. The advantages and disadvantages of each type of cooperation are summarized as follows.

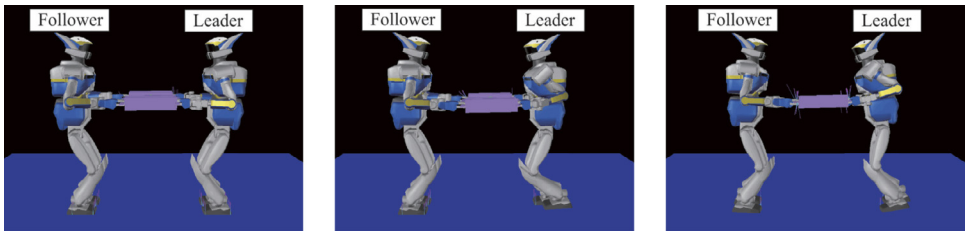

FIGURE 6.26 Simulation of the leader-follower-type cooperation.

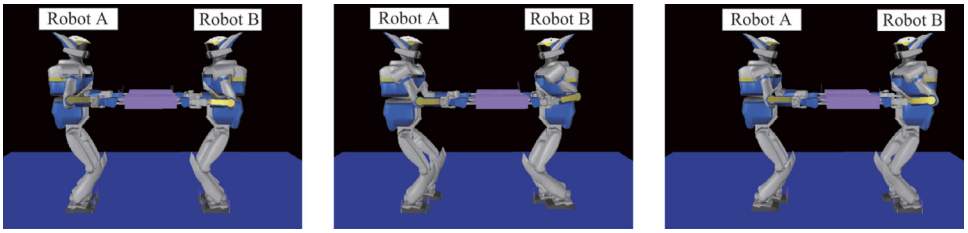

FIGURE 6.27 Simulation of the symmetry-type cooperation.

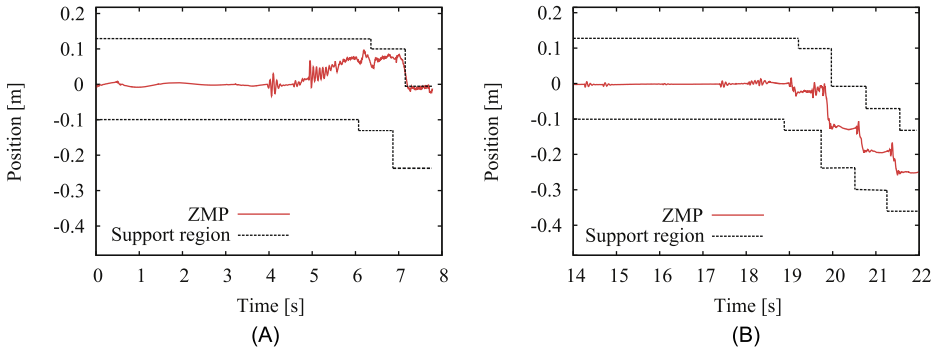

FIGURE 6.28 ZMP trajectory along the x-direction. (A) ZMP trajectory of the leader robot in the leader-follower-type cooperation. (B) ZMP trajectory of the robot B in the symmetry-type cooperation.

Leader-follower-type cooperation

Advantage: The control of the robots is decentralized. Therefore, there is no need of synchronization among the robots.

Disadvantage: The follower robots move based on the internal force generated at the object. Therefore, there is a time lag between the movements of the leader robot and those of the follower robots. The time lag may cause one or more of the robots to fall down.

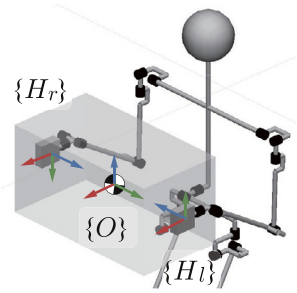

FIGURE 6.29 Object and hand coordinate frames. The contact joints at the hands impose unilateral planar constraints.

Symmetry-type cooperation

Advantage: All robots move synchronously. Ideally, there is no time lag among the robots. Thus, the risk of a robot to fall down is lower than that during leader-follower-type cooperation.

Disadvantage: The control of the robots is centralized. Therefore, synchronization among the robots is needed.

6.5 DUAL-ARM DYNAMIC OBJECT MANIPULATION CONTROL

Most tasks in the field of cooperative multifinger, dual-arm, and multirobot object manipulation are not time-critical. Such tasks can be handled with control methods based on the kinematic and kinetostatic relationships introduced in the previous sections of this chapter. There are, however, time-critical tasks where the speed of manipulation matters. Such type of tasks require a dynamics-based object manipulation control method. The control approach to be introduced in the remainder of this section is based on the kinematic, kinetostatic, and dynamic models developed in the previous chapters of this work. The approach is general in the sense that unilateral constraints at the hand contact joints can be handled, in addition to the bilateral ones used in the previous sections.

6.5.1 Equation of Motion of the Object

Suppose a humanoid robot grasps a rigid-body object with its hands s.t. *unilateral* plane contacts are established, as shown in Fig. 6.29. The coordinate frames of the object and the hands contacts, $\{O\}$ and $\{H_j\}$, respectively, are also shown in the figure. The equation of motion of the object is written in compact form as

$$\mathbb{M}_O \dot{\mathcal{V}}_O + \mathcal{C}_O + \mathcal{G}_O = \mathcal{F}_O. \tag{6.91}$$

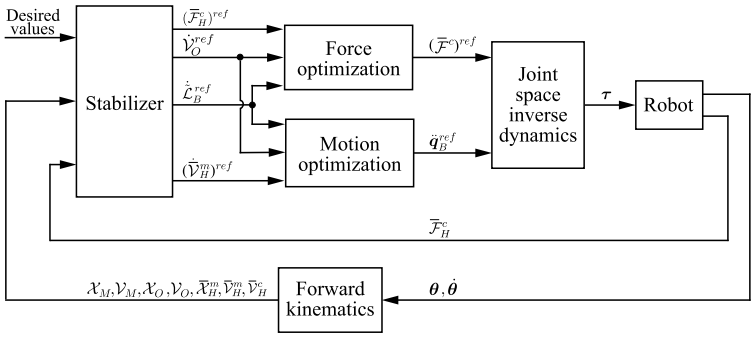

FIGURE 6.30 The motion/force controller based on the closed-chain formulation (cf. Fig. 5.29) is augmented with $\dot{\mathcal{V}}_O^{ref}$, the reference spatial acceleration for the desired object motion.

The expanded-form representation is

$$\begin{bmatrix} M_O \boldsymbol{E}_3 & \mathbf{0} \\ \mathbf{0} & \boldsymbol{I}_O \end{bmatrix} \dot{\mathcal{V}}_O + \begin{bmatrix} \mathbf{0} \\ \boldsymbol{\omega}_O \times \boldsymbol{I}_O \boldsymbol{\omega}_O \end{bmatrix} + \begin{bmatrix} M_O \boldsymbol{a}_g \\ \mathbf{0} \end{bmatrix} = -\mathbb{C}_{cO}(\boldsymbol{q}_H) \begin{bmatrix} \overline{\mathcal{F}}_{H_r}^c \\ \overline{\mathcal{F}}_{H_l}^c \end{bmatrix}. \tag{6.92}$$

Here M_O, $\boldsymbol{I}_O$ denote the mass and inertia tensor w.r.t. the CoM of the object, $\boldsymbol{\omega}_O$ is its angular velocity; $\mathbb{C}_{cO}(\boldsymbol{q}_H)$ is the contact map for the hands. Note the minus sign in the term on the r.h.s. It appears since the hand contact wrenches balance the *impressed* net wrench on the object, $\mathcal{F}_O$.

6.5.2 Controller

Dynamic object manipulation capabilities can be ensured with the dynamic motion/force controller introduced in Section 5.12.1. To this end, the controller in Fig. 5.29 is augmented as follows (see Fig. 6.30). First, the reference spatial acceleration for the object motion is defined as

$$\dot{\mathcal{V}}_O^{ref} = \begin{bmatrix} \dot{\boldsymbol{v}}_O^{ref} \\ \dot{\boldsymbol{\omega}}_O^{ref} \end{bmatrix} = \begin{bmatrix} \dot{\boldsymbol{v}}_O^{des} + K_{v_O} \dot{\boldsymbol{e}}_{p_O} + K_{p_O} \boldsymbol{e}_{p_O} \\ \dot{\boldsymbol{\omega}}_O^{des} + K_{\omega_O} \boldsymbol{e}_{\omega_O} + K_{o_O} \boldsymbol{e}_{o_O} \end{bmatrix}. \tag{6.93}$$

Here $\dot{\boldsymbol{v}}_O^{des}$ and $\dot{\boldsymbol{\omega}}_O^{des}$ are the desired linear and angular accelerations of the object, $\boldsymbol{e}_{\omega_O} = \boldsymbol{\omega}_O^{des} - \boldsymbol{\omega}_O$ denotes the error in the angular velocity, and $\boldsymbol{e}_{p_O}$ and $\boldsymbol{e}_{o_O}$ are the position and orientation errors, the latter defined by the preferable parametrization. The $K_{(\circ)}$ quantities stand for PD feedback gains. It is assumed here that the current 6D position and twist of the object are known, either calculated via the forward kinematics or measured.

Second, in the null-space prioritization scheme of the *motion optimization component* (see Fig. 5.30), an additional level is added in the hierarchy to account for the motion constraints in the independent closed loop formed by the hands and the object and for the motion of the object. This is shown in Fig. 6.31. Altogether, there are now four subtasks of priority.

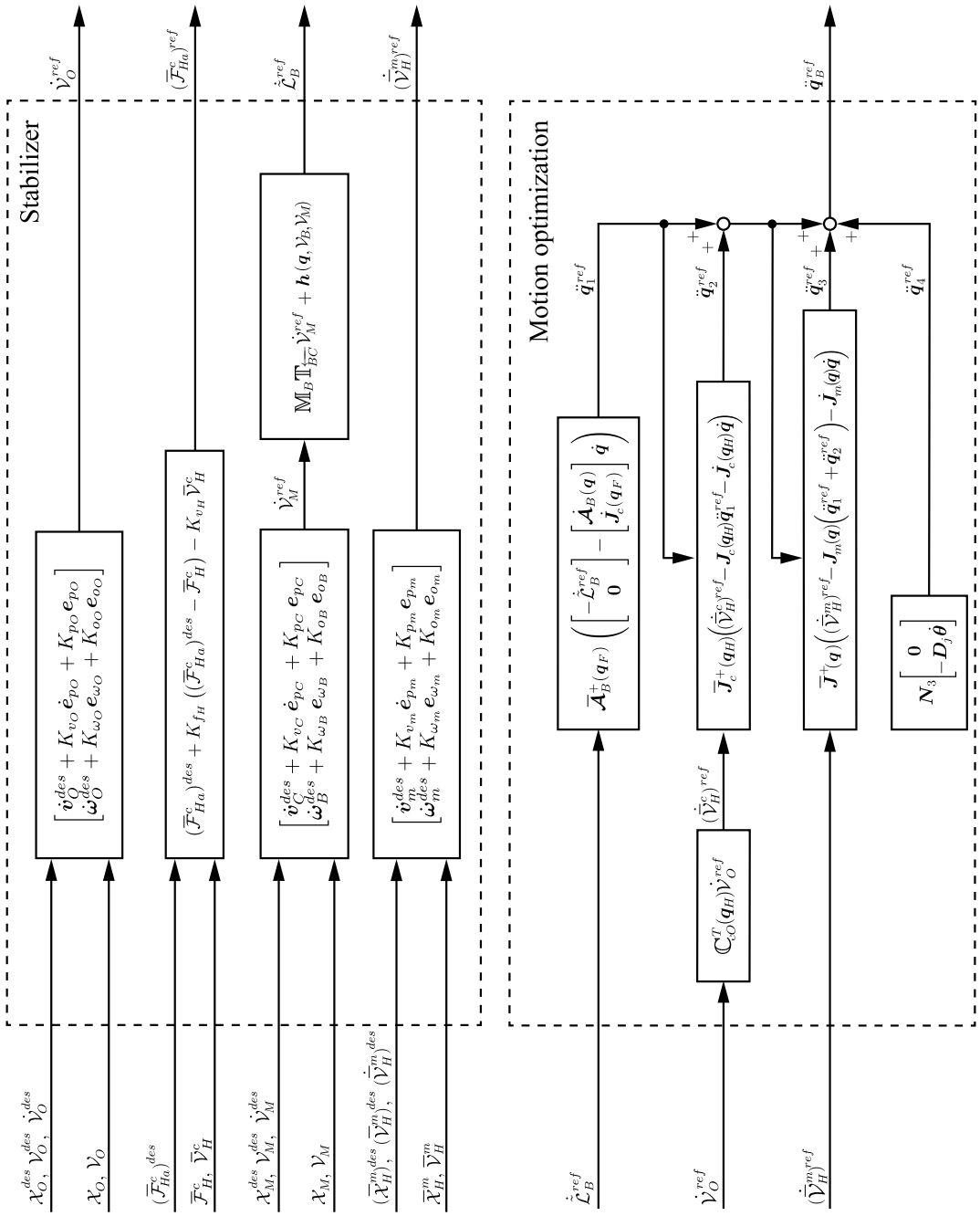

FIGURE 6.31 The equations used in the Stabilizer and Motion optimization blocks in Fig. 6.30.

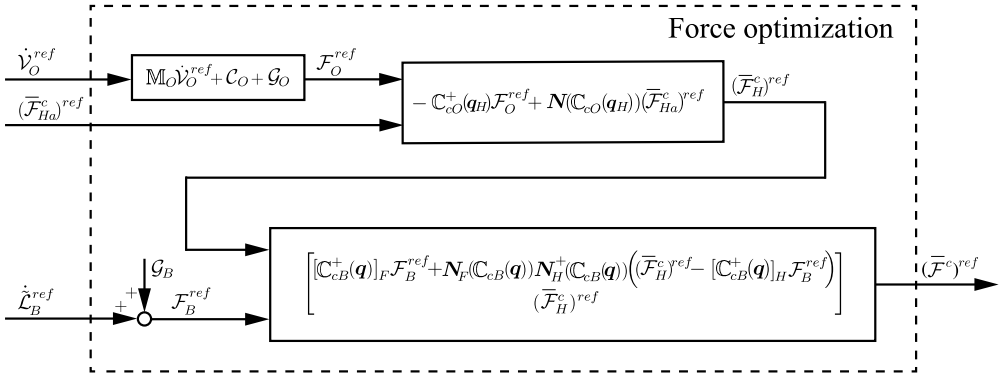

FIGURE 6.32 The equations used in the Force optimization block in Fig. 6.30.

The highest priority is for the balance control subtask ($\ddot{\boldsymbol{q}}_1$), the second highest for the object motion ($\ddot{\boldsymbol{q}}_2$), the third for the motion in the unconstrained (mobility) directions ($\ddot{\boldsymbol{q}}_3$), and the fourth for the self-motion ($\ddot{\boldsymbol{q}}_4$), in the form of joint-space damping in this case.

Third, the *wrench distribution problem for the hands* is solved in accordance with (3.66). The conventional force/moment control law

$$(\overline{\mathcal{F}}_{Ha}^c)^{ref} = (\overline{\mathcal{F}}_{Ha}^c)^{des} + K_{f_H}\left((\overline{\mathcal{F}}_{Ha}^c)^{des} - \overline{\mathcal{F}}_H^c\right) - K_{v_H}\overline{\mathcal{V}}_H^c, \tag{6.94}$$

which also appears in the controller in Fig. 5.29, is used here to squeeze the object with a desired force determined by $(\overline{\mathcal{F}}_{Ha}^c)^{des}$. This is done within the null space of the object contact map, $\mathcal{N}(\mathbb{C}_{cO})$, as apparent from Fig. 6.32. In this way, an appropriate internal wrench control can be ensured to enforce the contact wrench cone constraints.

The performance of the controller is examined with a dynamic object motion task simulated with a small-size humanoid robot.[2] An object of mass $M_O = 0.5$ kg and inertia tensor $\boldsymbol{I}_O = \text{diag}(1.92,\ 0.833,\ 1.92) \times 10^{-3}$ kgm^2 is grasped by the robot, lifted a bit, then shaken strongly, first in the x-, then in the y- and z-directions, followed by three consecutive rotations around the same axes and in the same order. The results are shown in graphical form in Fig. 6.33 and in Video 6.5-1 [23].

The desired position, velocity, orientation and angular velocity of the object are displayed in the upper row in Fig. 6.33. From the arm joint velocity graphs it can be confirmed that the motion is quite fast, indeed. The hand force graphs are presented in the local coordinate frames. They show that an internal (squeezing) force of 10 N is applied in the z-direction that

[2] The parameters of the model were derived from a HOAP-2 robot [4] (see Section A.2).

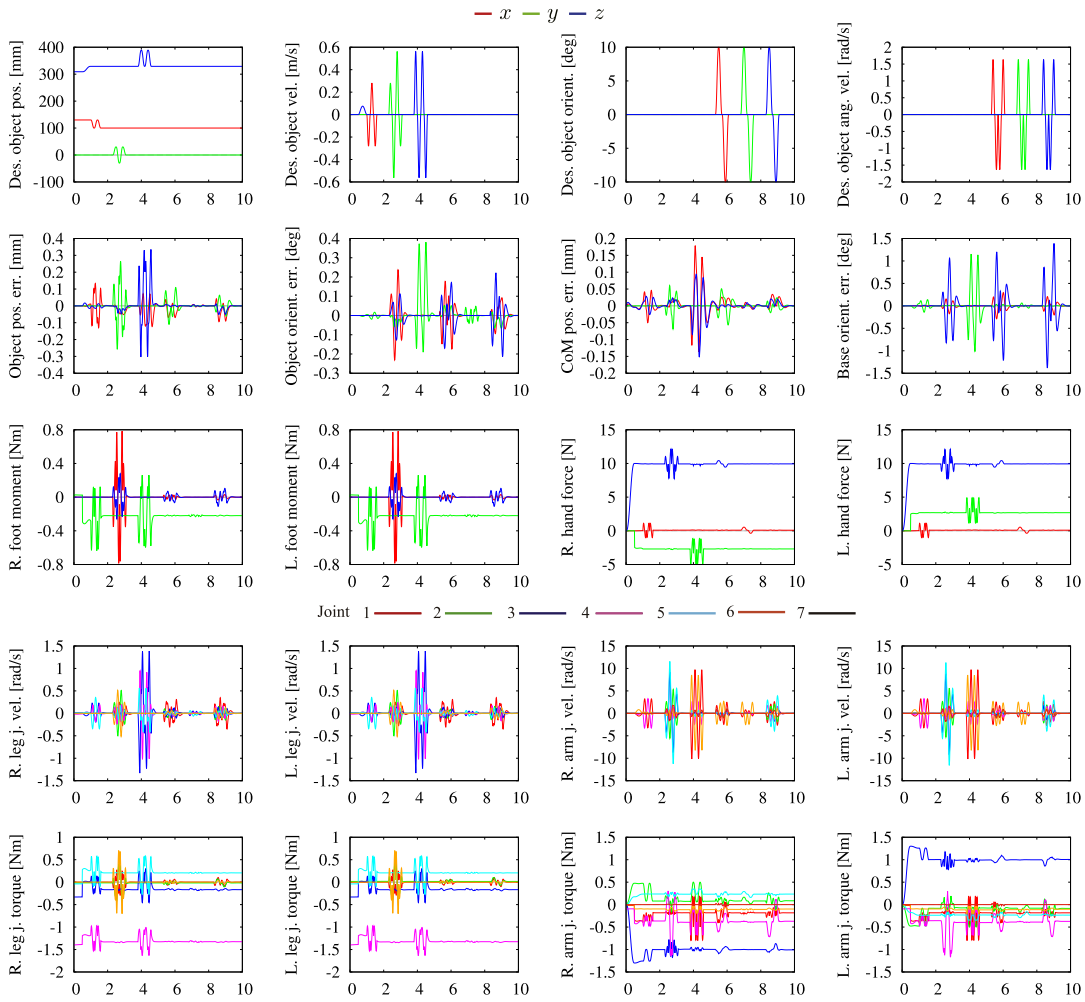

FIGURE 6.33 Results from a dynamic object-motion simulation task. The object is grasped, lifted a bit, then shaken strongly in the x-, y- and z-directions, and finally, rotated around these axes. The internal (squeezing) force prevents the object from slipping. The hand force graphs are presented in the local (sensor) frames. All other workspace related quantities are shown w.r.t. the world frame.

penetrates the object. In the world coordinate frame, this is the y-direction. From the error graphs for the object position/orientation, the CoM and the base rotation (the second row in Fig. 6.33) it is apparent that the performance is quite satisfactory since the errors are relatively small.

It should be noted that, in practice, the inertia tensor of the object may be unknown. The object mass can be estimated with measurements from the force/torque sensors in the wrists. The object dynamics (6.91) can then be reduced by ignoring the inertia and nonlinear wrench

components. The performance of the controller is quite robust w.r.t. the object dynamics reduced in this way.

References

[1] D.J. Agravante, A. Cherubini, A. Bussy, P. Gergondet, A. Kheddar, Collaborative human-humanoid carrying using vision and haptic sensing, in: Proceedings of IEEE International Conference on Robotics and Automation, 2014, pp. 607–612.

[2] A. Bicchi, On the closure properties of robotic grasping, The International Journal of Robotics Research 14 (1995) 319–334.

[3] F. Caccavale, P. Chiacchio, A. Marino, L. Villani, Six-dof impedance control of dual-arm cooperative manipulators, IEEE/ASME Transactions on Mechatronics 13 (2008) 576–586.

[4] Fujitsu, Miniature Humanoid Robot HOAP-2 Manual, 1st edition, Fujitsu Automation Co., Ltd, 2004 (in Japanese).

[5] S. Hayati, Hybrid position/force control of multi-arm cooperating robotics, in: Proceedings of IEEE International Conference on Robotics and Automation, 1986, pp. 82–89.

[6] D. Heck, D. Kostić, A. Denasi, H. Nijmeijer, Internal and external force-based impedance control for cooperative manipulation, in: Proceedings of European Control Conference, 2013, pp. 2299–2304.

[7] Y. Hirata, T. Sawada, Z.-D. Wang, K. Kosuge, Leader-follower type motion control algorithm of multiple mobile robots with dual manipulators for handling a single object in coordination, in: Proceedings of IEEE International Conference on Intelligent Mechatronics and Automation, 2004, pp. 362–367.

[8] S. Kajita, H. Hirukawa, K. Harada, K. Yokoi, Introduction to Humanoid Robotics, Springer Tracts in Advanced Robotics (STAR), Springer, 2014.

[9] S. Kajita, F. Kanehiro, K. Kaneko, K. Fujiwara, K. Harada, K. Yokoi, H. Hirukawa, Biped walking pattern generation by using preview control of zero-moment point, in: Proceedings of IEEE International Conference on Robotics and Automation, 2003, pp. 1620–1626.

[10] F. Kanehiro, K. Fujiwara, S. Kajita, K. Yokoi, K. Kaneko, H. Hirukawa, Y. Nakamura, K. Yamane, Open architecture humanoid robotics platform, in: 2002 IEEE International Conference on Robotics and Automation, IEEE, 2002, pp. 24–30.

[11] K. Kaneko, F. Kanehiro, S. Kajita, H. Hirukawa, T. Kawasaki, M. Hirata, K. Akachi, T. Isozumi, Humanoid robot HRP-2, in: IEEE International Conference on Robotics and Automation, Proceedings, vol. 2, ICRA '04, 2004, 2004.

[12] A. Konno, Cooperative object handling by four humanoid robots, 2016 (Video clip), https://doi.org/10.1016/B978-0-12-804560-2.00013-4.

[13] Y. Kume, Y. Hirata, Z.-D. Wang, K. Kosuge, Decentralized control of multiple mobile manipulators handling a single object in coordination, in: Proceedings of IEEE/RSJ International Conference on Intelligent Robots and Systems, 2002, pp. 2758–2763.

[14] Z. Li, S. Deng, C.Y. Su, T. Chai, C. Yang, J. Fu, Decentralized control of multiple cooperative manipulators with impedance interaction using fuzzy systems, in: Proceedings of IEEE International Conference on Information and Automation, 2014, pp. 665–670.

[15] M.T. Mason, Mechanics of Robotic Manipulation, Intelligent Robotics and Autonomous Agents Series, A Bradford Book, 2001.

[16] R.M. Murray, Z. Li, S.S. Sastry, A Mathematical Introduction to Robotic Manipulation, CRC Press, 1994.

[17] E. Nakano, S. Ozaki, T. Isida, I. Kato, Cooperational control of the anthropomorphous manipulator 'MELARM', in: Proceedings of 4th International Symposium of Industrial Robots, 1974, pp. 251–260.

[18] P. Pagilla, M. Tomizuka, Hybrid force/motion control of two arms carrying an object, in: Proceedings of American Control Conference, 1994, pp. 195–199.

[19] R. Rastegari, S.A.A. Moosavian, Multiple impedance control of cooperative manipulators using virtual object grasp, in: 2006 IEEE Conference on Computer Aided Control System Design, 2006 IEEE International Conference on Control Applications, 2006 IEEE International Symposium on Intelligent Control, IEEE, 2006, pp. 2872–2877.

[20] F. Reuleaux, The Kinematics of Machinery, Macmillan, New York, 1875. Republished by Dover, New York, 1963.

[21] J.K. Salisbury, B. Roth, Kinematic and force analysis of articulated mechanical hands, Journal of Mechanisms, Transmissions, and Automation in Design 105 (1983) 35–41.
[22] S. Schneider, R. Cannon, Object impedance control for cooperative manipulation: theory and experimental results, IEEE Transactions on Robotics and Automation 8 (1992) 383–394.
[23] T. Shibuya, S. Sakaguchi, D. Nenchev, Dynamic object shaking, Robotic Life Support Laboratory, Tokyo City University, 2018 (Video clip), https://doi.org/10.1016/B978-0-12-804560-2.00013-4.
[24] B. Siciliano, O. Khatib (Eds.), Springer Handbook of Robotics, Springer, Berlin, Germany, 2008, pp. 671–700, Chapter 28.
[25] B. Siciliano, O. Khatib (Eds.), Springer Handbook of Robotics, Springer, Berlin, Germany, 2008, pp. 701–718, Chapter 29.
[26] J. Szewczyk, F. Plumet, P. Bidaud, Planning and controlling cooperating robots through distributed impedance, Journal of Robotic Systems 19 (2002) 283–297.
[27] M. Uchiyama, P. Dauchez, Symmetric kinematic formulation and non-master/slave coordinated control of two-arm robots, Advanced Robotics 7 (1993) 361–383.
[28] D. Williams, O. Khatib, The virtual linkage: a model for internal forces in multi-grasp manipulation, in: 1993 IEEE International Conference on Robotics and Automation, 1993, pp. 1025–1030.
[29] M.-H. Wu, A. Konno, S. Ogawa, S. Komizunai, Symmetry cooperative object transportation by multiple humanoid robots, in: Proceedings of IEEE International Conference on Robotics and Automation, Hong Kong, China, 2014, pp. 3446–3451.
[30] M.-H. Wu, A. Konno, M. Uchiyama, Cooperative object transportation by multiple humanoid robots, in: Proceedings of IEEE/SICE International Symposium on System Integration, Kyoto, Japan, 2011, pp. 779–784.
[31] M.-H. Wu, S. Ogawa, A. Konno, Symmetry position/force hybrid control for cooperative object transportation using multiple humanoid robots, Advanced Robotics 30 (2016) 131–149.
[32] K. Yokoyama, H. Handa, T. Isozumi, Y. Fukase, K. Kaneko, F. Kanehiro, Y. Kawai, F. Tomita, H. Hirukawa, Cooperative works by a human and a humanoid robot, in: Proceedings of IEEE International Conference on Robotics and Automation, 2003, pp. 2985–2991.
[33] T. Yoshikawa, X.Z. Zheng, Coordinated dynamic control for multiple robot manipulators handling an object, in: Proceedings of Fifth International Conference on Advanced Robotics, 1991, pp. 579–584.